October 1989

WRRI Report No. 245

ANALYSIS OF SOIL-WATER MOVEMENT ON A SANDY HILLSLOPE

Technical Completion Report
Project No. 1423660

ANALYSIS OF SOIL-WATER MOVEMENT ON A SANDY HILLSLOPE

By

James T. McCord
Graduate Research Assistant

and

Daniel B. Stephens
Department of Geoscience and
Research and Economic Development Division
New Mexico Institute of Mining and Technology

TECHNICAL COMPLETION REPORT
Project Numbers: 14-08-0001-G1130, 1423660

October 1989

New Mexico Water Resources Research Institute

The research on which this report is based was financed in part by the U.S. Department of the Interior, Geological Survey, through the New Mexico Water Resources Research Institute.

DISCLAIMER

The purpose of Water Resources Research Institute technical reports is to provide timely outlet for research results obtained on projects supported in whole or in part by the institute. Through these reports, we are promoting the free exchange of information and ideas, and hope to stimulate thoughtful discussion and actions that may lead to resolution of water problems. The WRRI, through peer review of draft reports, attempts to substantiate the accuracy of information contained in its reports, but the views expressed are those of the authors and do not necessarily reflect those of WRRI or its reviewers. Contents of this publication do not necessarily reflect the views and policies of the U.S. Department of Interior, nor does mention of trade names or commercial products constitute their endorsement by the United States government.

ABSTRACT

This report describes a series of detailed soil-water tracer experiments conducted in a natural landscape and investigates three distinct approaches to numerically model the flow and transport behavior observed in the field experiments. These experimental and numerical results strongly suggest that current widely held views and commonly applied modeling approaches are flawed in many cases for unsaturated flow. The field experiments provide strong supporting evidence for a variable, state-dependent anisotropy in the hydraulic conductivity of an unsaturated medium. This phenomenon has been previously postulated in a number of independent theoretical and experimental investigations. In general, these studies identify layered heterogeneity as a primary cause of the macroscopic anisotropy. In addition, we show how hysteresis-enhanced moisture content variations can cause a texturally homogeneous porous media profile to behave anisotropically under transient unsaturated conditions. Recognizing that both of these factors (layered heterogeneity and capillary hysteresis) contribute the anisotropic behavior observed in the tracer experiments, we attempt to quantify the relative magnitude of their contributions in a numerical modeling investigation. For the numerical modeling study we use a finite element flow and transport code, and we introduce a simple procedure for incorporating variable anisotropy into the model. Based on a first-order sensitivity analysis of a stochastic estimator of variable anisotropy (Yeh et al.,1985b), we make anisotropy a single-valued function of pressure head in our implementation of this phenomenom. To determine the relative magnitude of textural heterogeneity and capillary hysteresis as contributors to the observed macroscopic anisotropy, we employ a diagnostic modeling approach. The results of the diagnostic modeling study indicate that textural heterogeneity is by far the most important contributor to the variable macroscopic anisotropy observed at the field site, and they further show that the variable anisotropy approach is well suited to modeling field-scale problems. Subsequently, a sensitivity analysis is performed to determine how climate, geologic and topographic structure, and media lithology affect flow and transport behavior when soils were specified to have a variable macroscopic anisotropy. The results of this study clearly indicate that variable state-dependent anisotropy is a real and significant process at the field site and that modeling with consideration of variable anisotropy strongly affects model predictions. There is a practical need to further investigate this variable anisotropy phenomenom and determine how it may affect our understanding of a wide variety of hydrological processes.

Key words: Soil moisture movement, unsaturated soils, ground water

TABLE OF CONTENTS

LIST OF FIGURES

LIST OF TABLES

INTRODUCTION

At most locations on our planet, meteoric waters and anthropogenically applied (or spilled) fluids must travel through a variably saturated vadose zone before they can enter underlying aquifers. In some locations the vadose zone is on the order of decimeters thick; in others its thickness may be measured in hundreds of meters. Unfortunately, some of man's land use practices over the centuries (particularly in the most recent century) have resulted in pollutants traveling through the vadose zone and contaminating many aquifers which we rely upon for our drinking water supply. Typically the contamination results from ignorance and/or carelessness in (1) the application of agricultural chemicals, and (2) the storage and disposal of waste products. Recent years have witnessed the growth of the idea that the vadose zone may be one of the best receptacles for many of our wastes, if such disposal is carried out in the appropriate careful and responsible manner. This is particularly true for arid lands. Perhaps the best example of the "vadose zone as a waste receptacle" philosophy is the selection of Yucca Mountain, Nevada as the United State's top candidate for disposal of commercial high–level radioactive wastes. Given that many of man's land use practices result in the introduction of noxious substances on the ground surface, and given that some of our most deadly wastes are being deliberately buried in the vadose zone, it is vital that we develop the best possible conceptual and mathematical models for fluid flow in unsaturated geologic media.

In the past couple of decades an increasing number of studies have investigated the impact of media heterogeneities on the flow and transport processes. These problems have been investigated in field and laboratory experiments, as well as analytically by

applying existing mathematical models to porous media whose heterogeneities can be deterministically described (Bouwer, 1969; Philip, 1974). A number of studies (Nielsen et al., 1978; Byers and Stephens, 1983) have recognized and demonstrated that in the real world, geologic media heterogeneities are next to impossible to completely define and that the application of geostatistics may yield useful parameters for describing media spatial variability. Others have applied existing models of flow and transport with explicit recognition of random media heterogeneity to obtain new stochastic mathematical models (Andersson and Shapiro, 1983; Dagan and Bresler, 1983; Mualem, 1984; Yeh et al., 1985a). One of the most important findings of the stochastic studies for unsaturated soils is the result of Gelhar and his associates (Yeh et al., 1985a,b,c; Mantoglou and Gelhar, 1987a,b,c), which suggests that the hydraulic conductivity anisotropy (ratio of the major axis to the minor axis of the conductivity tensor) will vary as the hydraulic state (mean pressure head, and spatial and temporal head gradients) of the media varies.

Variable, state-dependent anisotropy in unsaturated soils is an effective, large-scale (macroscopic) flow property which results from media textural heterogeneities at a smaller scale. The same type of behavior was predicted in independent studies by Zaslavsky and Sinai (1981a,b,c,d) and Mualem (1984). All of these studies are theoretical in nature and they provide no substantive field validations of state-dependent anisotropy. However, some of the papers (Zaslavsky and Sinai, 1981a; Yeh et al., 1985c; Mantoglou and Gelhar, 1987c) do cite field examples which indirectly suggest that this phenomena may be important at some sites.

With direct field evidence for state–dependent anisotropy lacking, we decided to con-

duct a series of tracer experiments in a natural field setting, with simultaneous hydraulic head monitoring. This paper will describe those experiments in detail. We believe these experiments substantially validate (or at least provide strong evidence for) the concept of state–dependent anisotropy. In addition to the textural heterogeneity causes discussed by Maulem (1984), Yeh et al. (1985c), and Mantoglou and Gelhar (1987), we feel there is another important factor which contributes to the anisotropic behavior observed in the tracer experiments. We term this other contributing factor "moisture–dependent variations in hydraulic conductivity." We will show how this phenomena can cause texturally homogeneous materials to behave as hydraulically anisotropic media when viewed at the field scale, and how hysteresis in the soil moisture characteristics tends to magnify this phenomena.

A major part of this paper investigates the implementation of variable state-dependent anisotropy in a numerical model of unsaturated flow. As was pointed out by Bear and Braester (1987), essentially all numerical models of unsaturated flow represent the effective hydraulic conductivity of an anisotropic porous medium as a product of the saturated hydraulic conductivity tensor k_{sij}, and the relative hydraulic conductivity K_r, which is a function of saturation S. The same relative conductivity function $K_r(S)$ is assumed to apply to all components of the effective hydraulic conductivity $K_{ij}(S)$; i.e., the magnitude of the anisotropy remains constant throughout the entire range of saturations. Based on the aforementioned theoretical and experimental studies, we join Bear and Braester (1987) in questioning the validity of this commonly used approach of handling anisotropy in variably saturated flow models.

The variable anisotropy expressions developed in the stochastic studies by Yeh et al. (1985b) and Mantoglou and Gelhar (1987c) indicate that anisotropy depends on a number of parameters which characterize the spatial variability of the heterogeneous porous media, as well as on the mean pressure head, and the spatial and temporal head gradients. Results of a first-order sensitivity analysis presented herein suggest that anisotropy is much more sensitive to the mean pressure head than to the direction or magnitude of the spatial head gradient for a broad range of typical field conditions. Furthermore a trial simulation of rapid wetting followed immediately by evaporation and drainage indicates that the influence of the temporal head gradient on the resulting flow system is relatively minor for systems with soil-water tension heads less than 0.5 bars. Given the results of the sensitivity analysis and the trial simulation, we suggest that in many cases the variable anisotropy may be adequately represented as a single-valued function of pressure head. Thus a simple, straight-forward, and general procedure for implementing variable anisotropy is introduced.

This procedure is employed to develop a variably saturated flow and transport code which allows for explicit consideration of moisture dependent anisotropy. The flow model is essentially an extension of the widely applied Richards equation approach. The code is written such that hysteresis in the soil moisture characteristics can also be accounted for. The resulting model is then used to simulate a variety of field situations. First the code is used in a series of diagnostic simulations which was designed to identify the primary cause of the anisotropic behavior observed in the field tracer experiments. The results of the diagnostic simulations indicate that heterogeneity in the soil properties played a much larger role than capillary hysteresis in causing the observed variable macroscopic

anisotropy. Next a series of sensitivity simulations were performed to investigate the impact of moisture-dependent anisotropy on unsaturated flow for a variety of climatic, geologic, and lithologic conditions. All of these simulations underline the importance of accounting for variable state-dependent anisotropy when modeling unsaturated flow and transport.

FIELD AND LABORATORY ANALYSES

In an anisotropic medium, if the hydraulic gradient direction does not coincide with one of the principal directions of the hydraulic conductivity tensor, there will be a non-colinearity of the net flux and hydraulic gradient directions. Therefore, detailed measurements of the gradient vector field and the resultant flux field should allow one to calculate the effective anisotropy of the porous media. Following this line of reasoning we performed a number of vadose zone tracer experiments in the shallow soils on a sandy hillslope at an arid site near Socorro, New Mexico. Simultaneous with the tracer experiments, detailed measurements of the subsurface hydraulic head and moisture content were collected.

Site Description

The site comprises an area of about 900 m^2 situated in the Sevilleta National Wildlife Refuge about 25 km north of Socorro, NM. The site lies on a small sand dune on the south side of the Rio Salado, an ephemeral braided tributary to the Rio Grande. A generalized location map is shown on Figure 1. The area receives about 20 cm of precipitation per

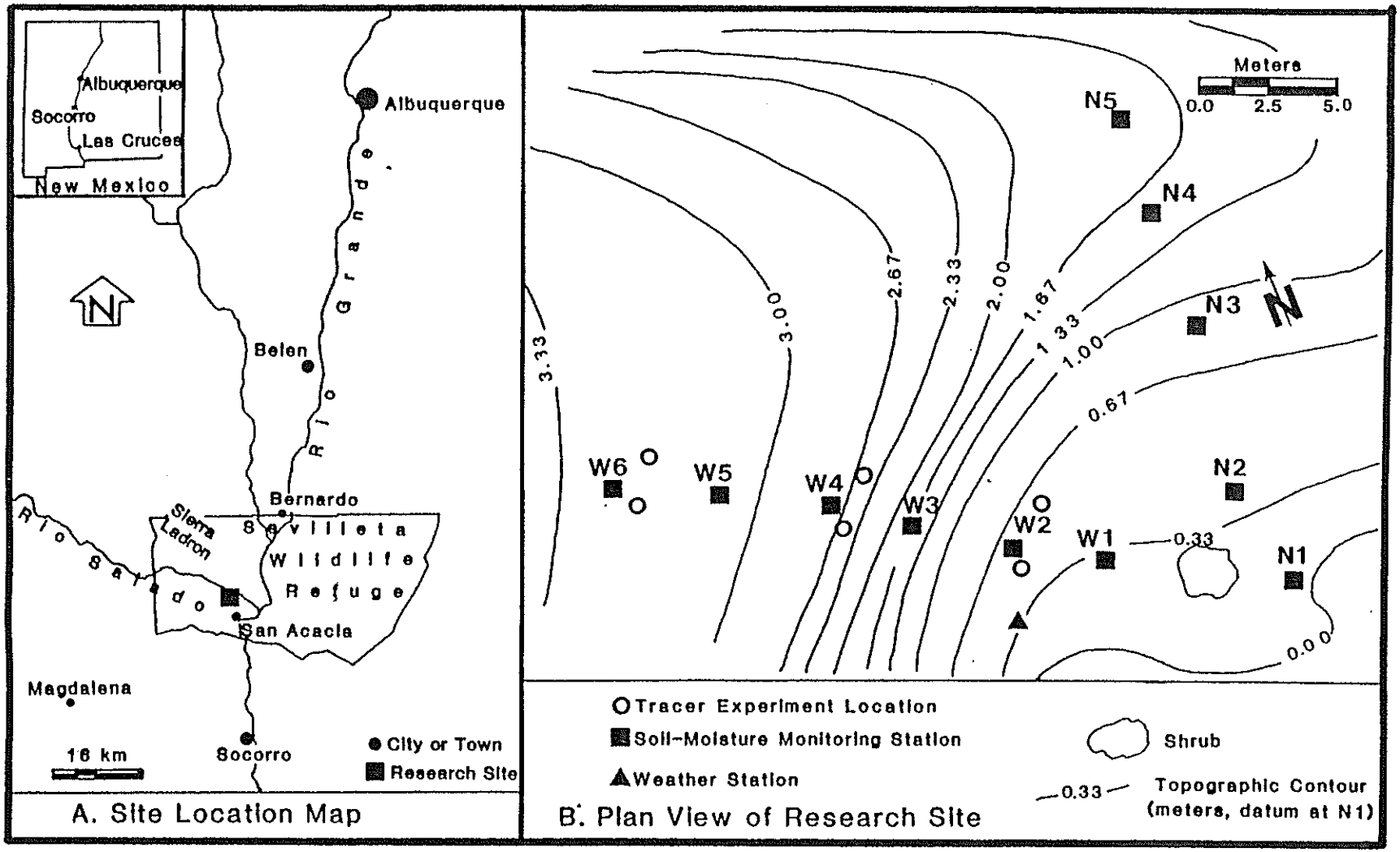

Figure 1. Location map and plan view of field experiment site.

year and the gross annual potential lake evaporation is about 178 cm. Figure 1 also presents a topographic map of the ground surface at the study location. Included with the topographic map is a layout of the subsurface monitoring equipment. The monitoring equipment is described subsequently in the Site Monitoring section.

The investigation reported here is based on a series of tracer experiments conducted along the east–west trending instrumentation transect. The dune surface topography along the north instrumentation transect varied dramatically as the sands shifted in response to the predominately north–south wind directions. Therefore, we did not conduct any experiments on the north transect. Along the west transect, the topography was much more stable and dune surface elevations did not change by more than 10 cm.

The surficial lithology consists of fine to medium, uniform sands to a depth of 6.5 meters, the maximum depth to which we sampled. Trenches excavated in the sand revealed no apparent fine–grained layers, although we could discern medium– to large–scale eolian cross– stratifications. The foreset beds were on the order of 1 to 3 millimeters thick and were oriented parallel to subparallel to the ground surface slope.

Site Monitoring

The instrumentation array included 11 soil–water monitoring stations, and a fully automated weather station (Figure 1). The weather station was composed of a temperature/relative humidity probe, a tipping bucket rain gage, a silicone pyronometer, and wind speed and wind direction sensors. Each of these instruments was connected to a microprocessor (Model 21X, Campbell Scientific Inc., Logan, Utah) which was programmed to sample data from each of the instruments continuously throughout the day. Each

soil–water monitoring station consisted of an aluminum tube advanced to a depth of 3 meters to provide access for a neutron probe to measure moisture content, and tensiometers installed in duplicate at depths of 30, 60, 90, 120, and 150 cm to permit hydraulic head measurements. We monitored the soil–water stations on a weekly basis. In addition, tensiometers also were installed at a depth of 244 cm at stations N1 and W2 to verify downward hydraulic gradients, and gypsum electrical resistance blocks were emplaced at 10, 20, and 30 cm depths at most stations on the west transect (W2 through W6) to provide hydraulic head estimates in the near–surface sands which often dry to tension heads which exceed the operation range of tensiometers. The gypsum blocks were also connected to the datalogger.

After all of the instrumentation was in place, we conducted a two–month long baseline monitoring program to test our monitoring array. Figure 2 shows the measured soil moisture and hydraulic head conditions on the west transect for three days in July, 1986. Given that climatic inputs at the soil surface are uniformly distributed in space at the transect scale, Figure 2 suggests that multidimensional unsaturated flow processes at the field site cause a highly variable moisture content distribution at depth. Once it was established that all of the equipment was operating properly, we commenced with the tracer tests.

Tracer Experiments

Six tracer experiments were performed on the west transect at three different topographic positions: on a relatively level position near the top of the slope (station W6), a sloping position near the middle of the transect (between stations W3 and W4), and a

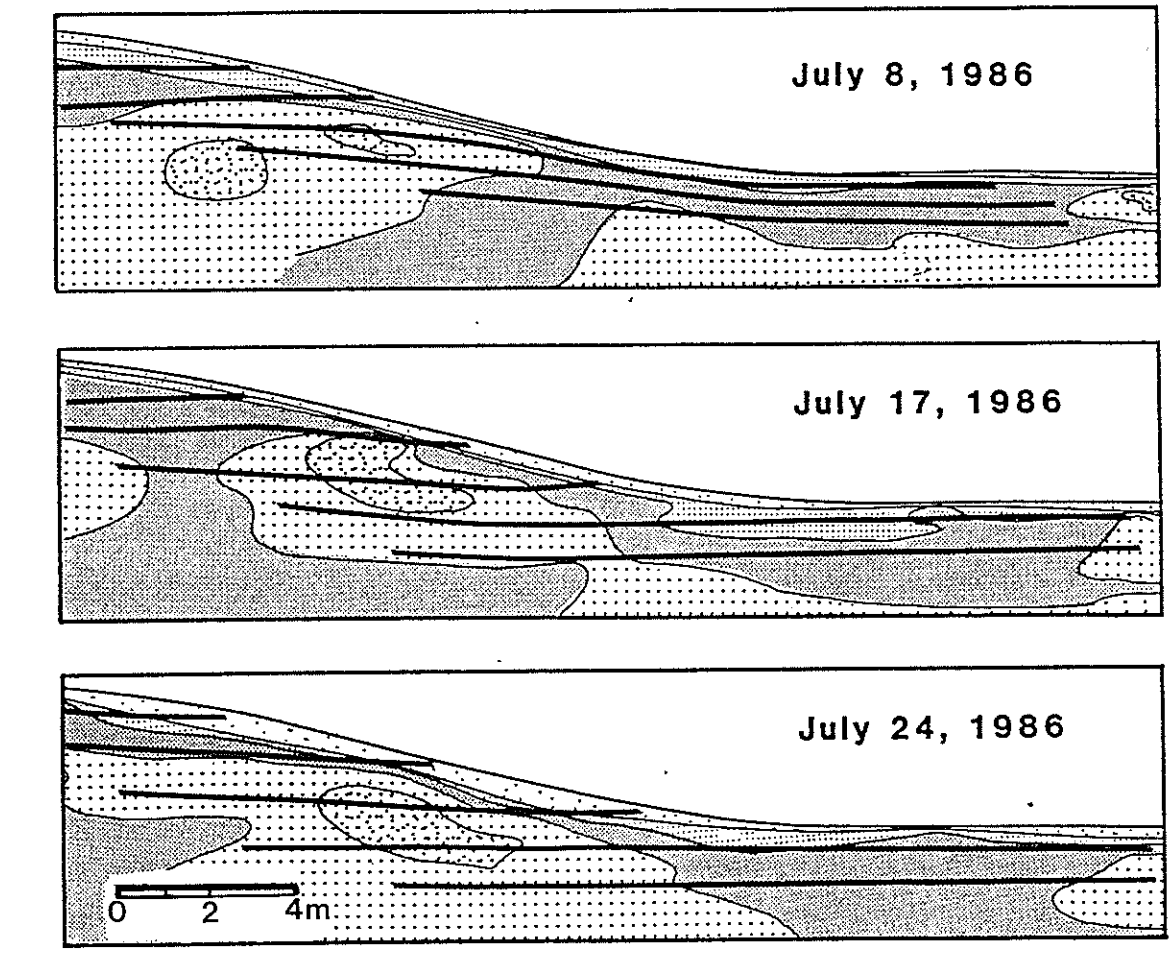

Fig. 2. Moisture content and total head fields observed at the field site for 3 days in July 1986.

level position at the base of the slope (station W2). We selected these locations for the experiments based on Zaslavsky and Sinai's (1981a,b) argument that the ground surface slope will have a significant effect on the magnitude of the horizontal components to flow. The location of each experiment is shown in the plan view presented in Figure 1. Tracers were buried at two different depths at each position: the tracers were buried at a 10 cm depth for the experiments conducted on the north side of the instrumentation transect (see Figure 1), and at a 40 cm depth for the experiments on the south side of the transect.

The tracer experiments were conducted as follows. At each selected position, a 30 cm long, narrow ($\simeq$ 3cm) trench was excavated perpendicular to the ground surface slope to the desired depth. A small amount (50 grams) of a dry bromide salt ($CaBr_2$) was then tremmied to the bottom of the excavation between two parallel metal plates. We distributed the bromide salt as evenly as possible along the bottom of the trench so that essentially we had a 30 cm long line source of tracer. Following precipitation, soils from each location were sampled along transects perpendicular and parallel to the line source. We sampled by driving 1.5 cm inner diameter thin-walled tubing into the soils. These continuous samples were subsequently sectioned in our laboratory, weighed, oven dried and reweighed. Next a known volume of distilled, de-ionized water was added to the dried samples. The resulting soil slurry was agitated to promote solute dissolution and a small volume of liquid was subsequently removed and analyzed for bromide concentration using an ion specific electrode. The sequence of precipitation and sampling events for the tracer experiments is summarized in Table 1.

Figures 3 through 9 present the tracer test results. Figure 3 shows Br^- concentration

TABLE 1

Sequence of Events for 1986 Tracer Experiments.

Date Tracer Emplaced	Precipitation mm depth/date	Date Sampled
Sept. 3	9.0/Sept. 8	-
	0.8/Sept. 10	-
	8.8/Sept. 13-15	-
	7.6/Sept. 23	-
	-	Sept. 25
	20.4/Oct. 5-6	-
	48.6/Oct. 10-12	Oct. 16

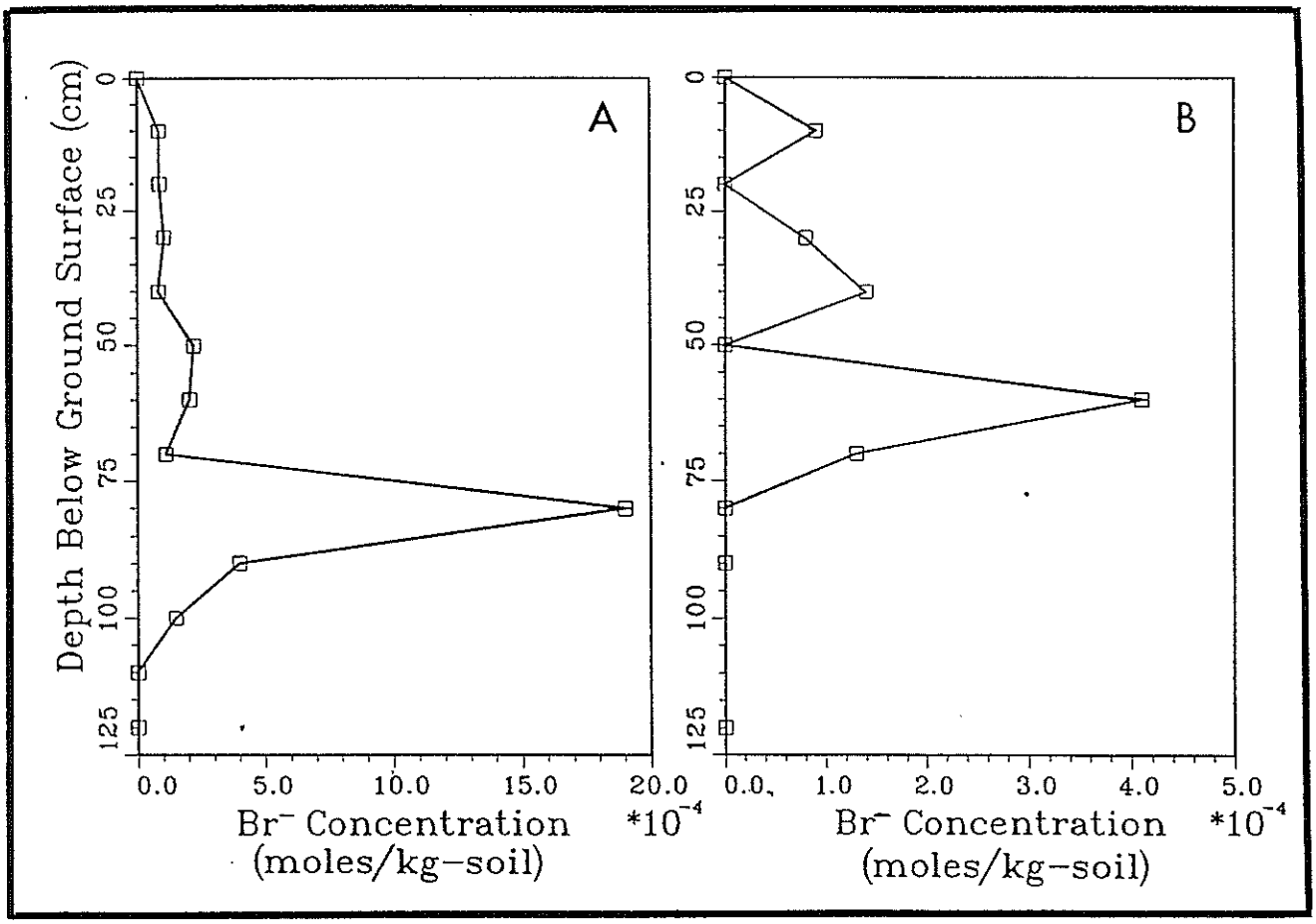

Fig. 3. Bromide concentration versus depth at two locations.
A. Tracer experiment W3s, samples obtained 50cm downslope from tracer source on 9/25/86;
B. Tracer experiment W3n, samples obtained 120cm downslope from source on 10/16/86.

versus depth at two locations, clearly demonstrating the highly variable tracer concentration profiles measured at most sampling locations. This variability may be due to both sampling and analytical errors, as well as fine scale variations in the vadose water flux rates. Figures 4 through 9 present profile views of solute plume contours derived from smoothed concentrations and plan views of solute contours obtained by integrating the concentrations over the depth sampled. The concentrations contoured in the profile views were obtained using the following weighted average process to smooth out irregularities in measured data:

$$C_s(i) = 1/4\,[C(i-1) + 2C(i) + C(i+1)] \tag{1}$$

where $C_s(i)$ is the smoothed concentration at depth i, $C(i)$ is the measured concentration at that depth, and $C(i \pm 1)$ is the measured concentration at the adjacent depths above and below i. Integrating the plumes in the plan view over the area covered, one can obtain an estimate of mass of bromide contained within each plume. Normalizing this mass with respect to mass originally emplanted gives an indication of the amount of tracer recovered. Tracer recovery percentages are presented in Table 2. Also shown in the profile view of Figures 4 through 9 are contours of average total head measured during the tracer experiment. Average values are presented rather than particular values for particular dates because the head remained relatively constant throughout the experiments (McCord, 1988).

Utilizing the tracer plume orientation in conjunction with the head measurements, one can estimate the effective anisotropy of the soil profile. Diffusion calculations indicate that advective transport dominates over diffusive transport in these experiments. Therefore one can use the plumes to infer components of the soil water flux in the directions

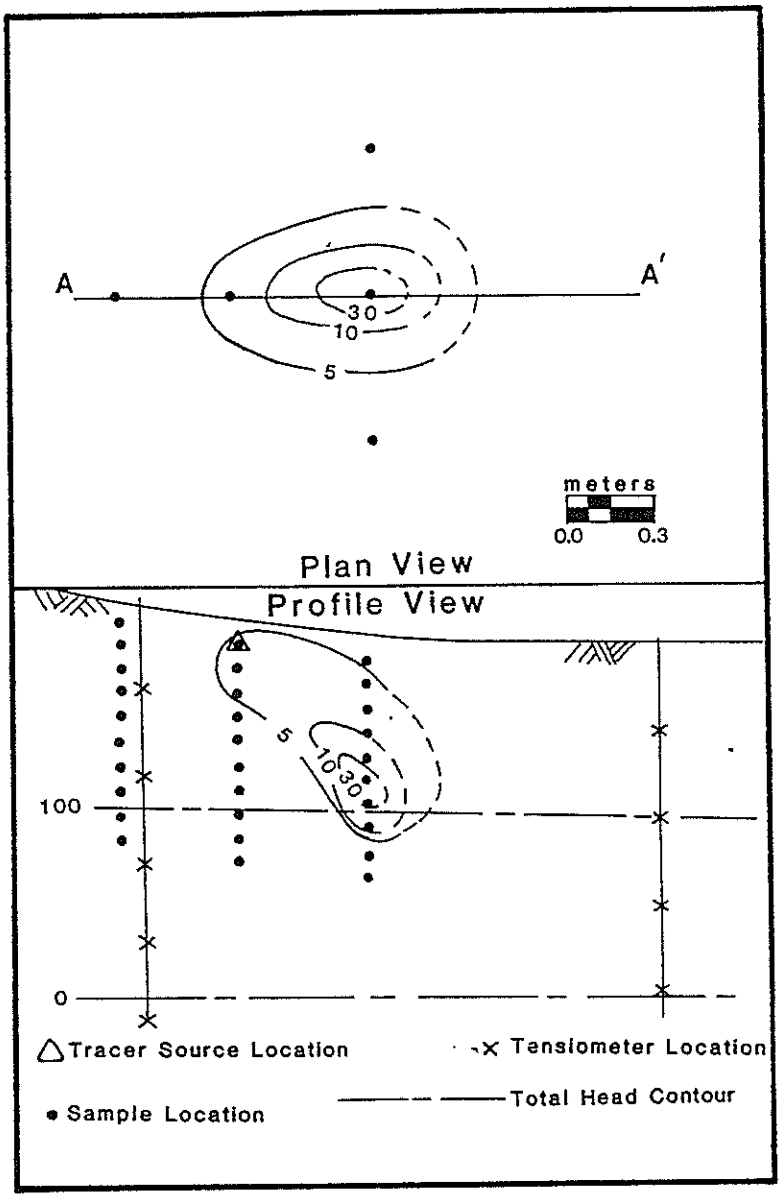

Fig. 4. Plan and profile views of solute plume from experiment where the tracer was planted at a 10cm depth just north of station W2. Tracer concentrations are given in (moles/kg-soil), and total head in (cm-water). Profile view taken along axis AA' shown in the plan view.

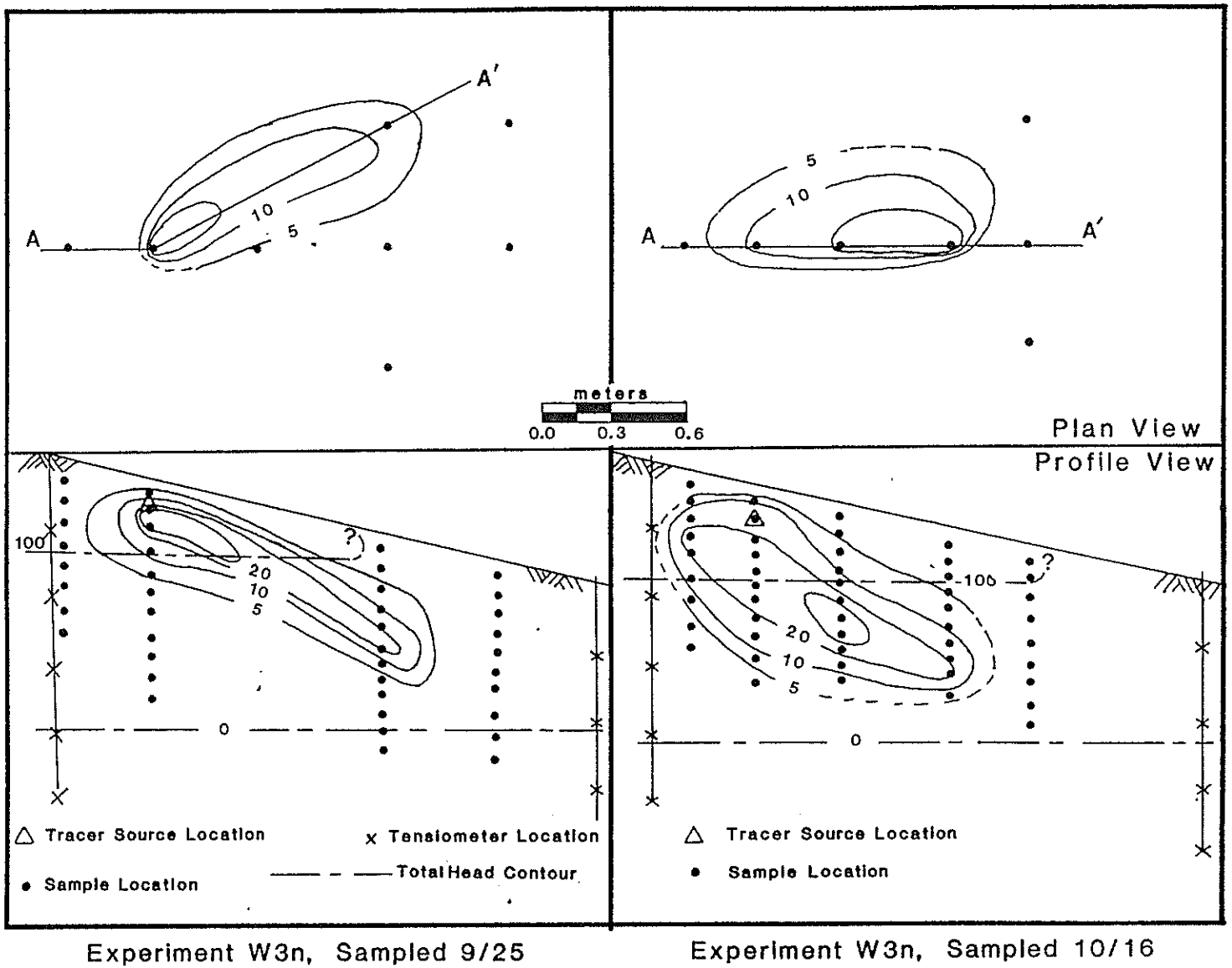

Fig. 5. Plan and profile views of solute plume from experiment where the tracer was planted at a 10cm depth just north of station W3. Tracer concentrations are given in (moles/kg-soil), and total head in (cm-water). Profile view taken along axis AA' shown in the plan view.

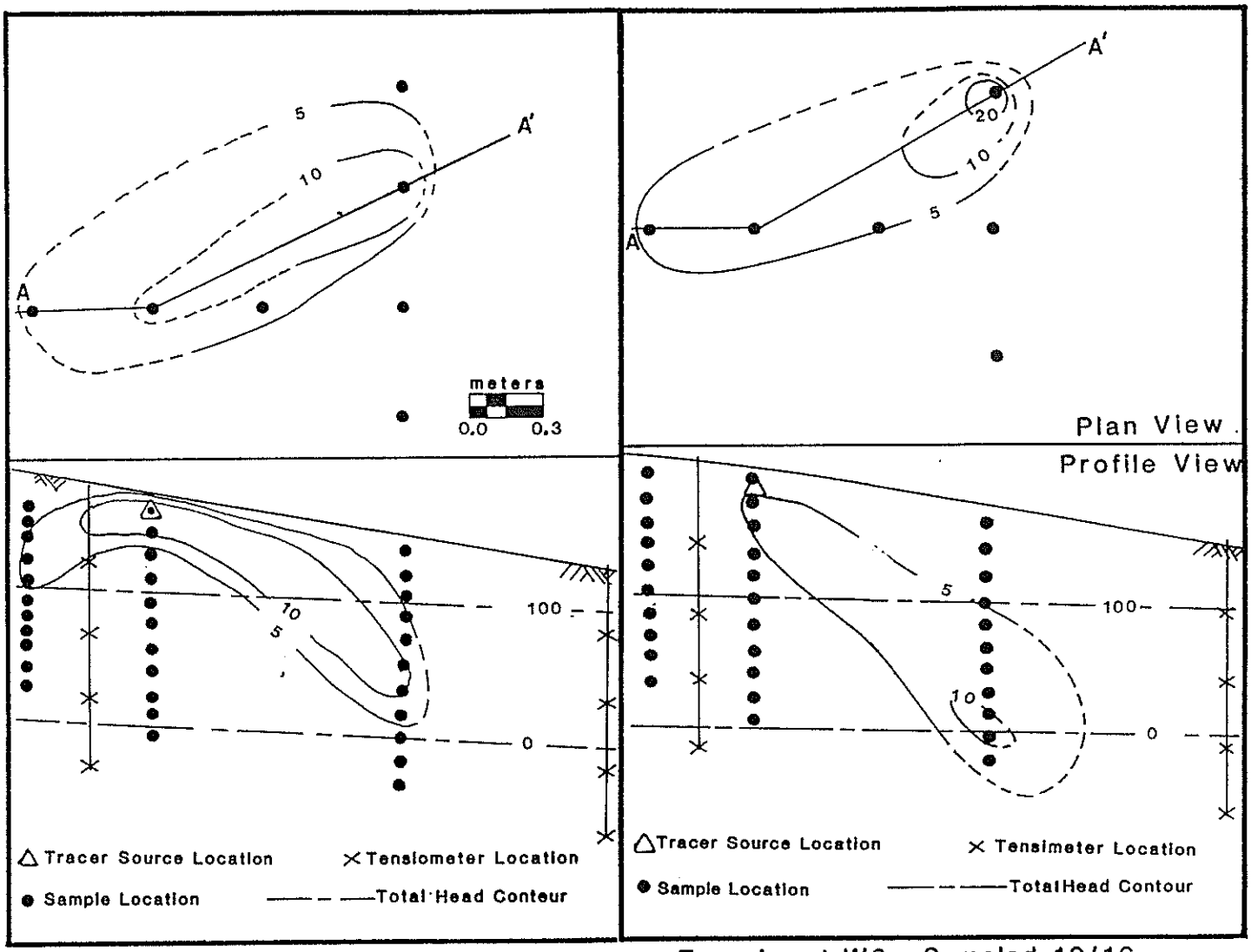

Fig. 6. Plan and profile views of solute plume from experiment where the tracer was planted at a 10cm depth just north of station W6. Tracer concentrations are given in (moles/kg-soil), and total head in (cm-water). Profile view taken along axis AA' shown in the plan view.

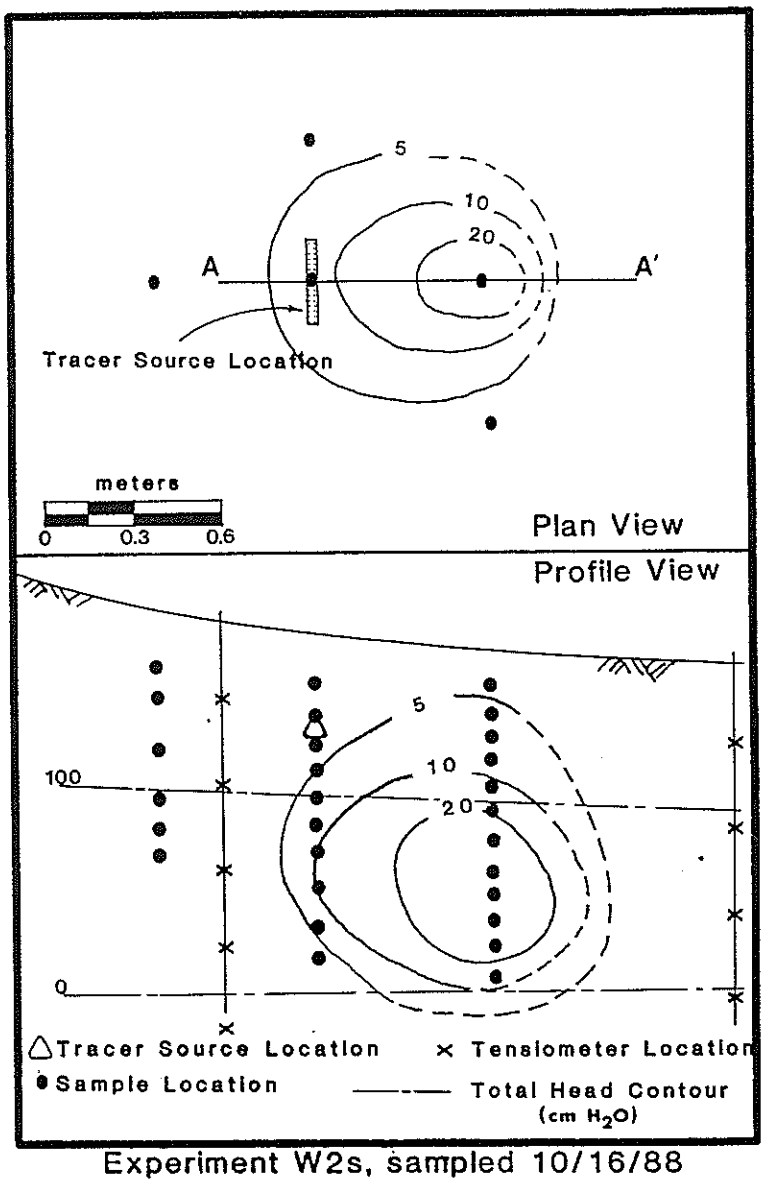

Fig. 7. Plan and profile views of solute plume from experiment where the tracer was planted at a 40cm depth just south of station W2. Tracer concentrations are given in (moles/kg-soil), and total head in (cm-water). Profile view taken along axis AA' shown in the plan view.

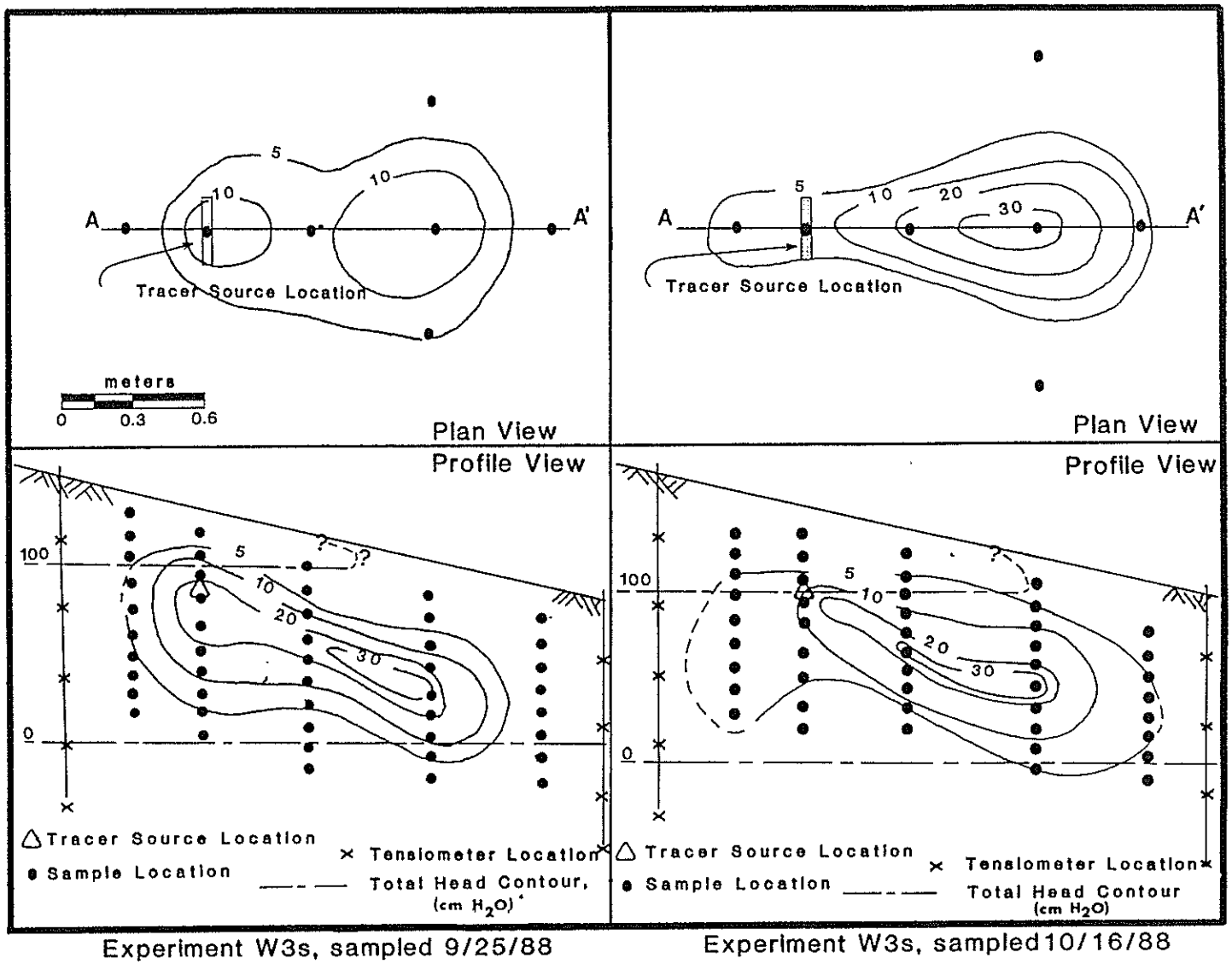

Fig. 8. Plan and profile views of solute plume from experiment where the tracer was planted at a 40cm depth just south of station W3. Tracer concentrations are given in (moles/kg-soil), and total head in (cm-water). Profile view taken along axis AA' shown in the plan view.

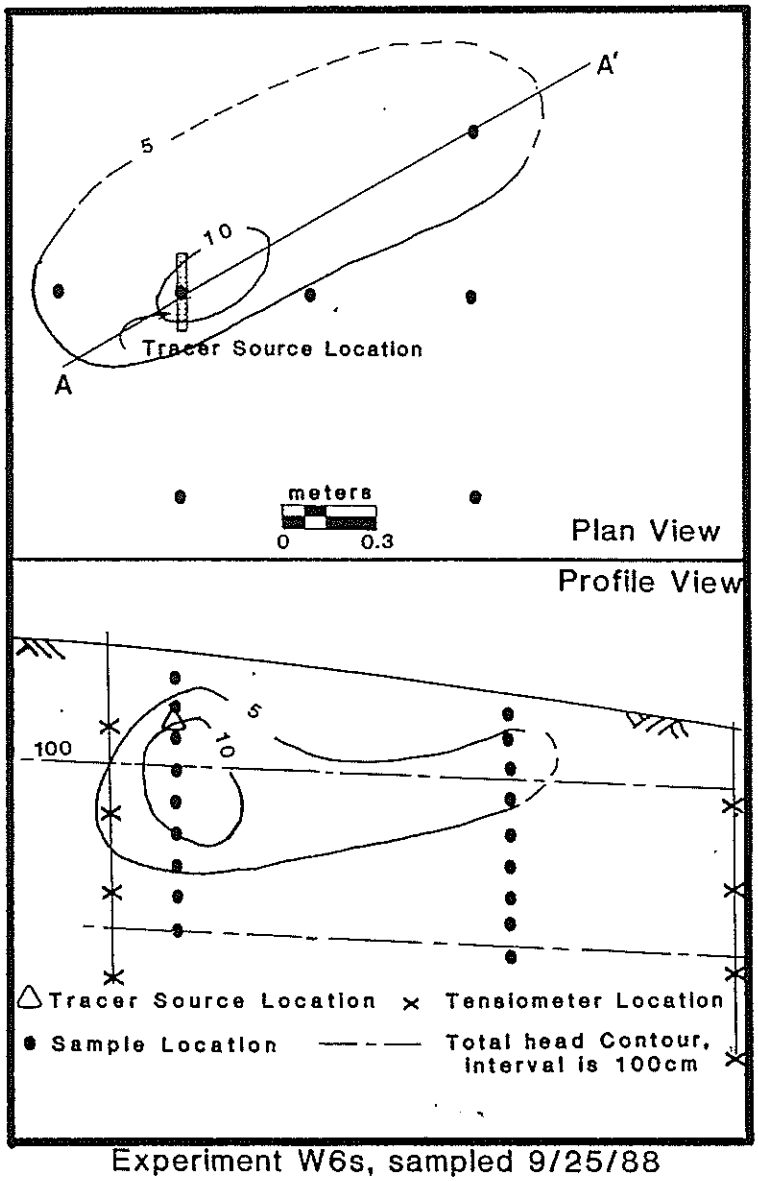

Fig. 9. Plan and profile views of solute plume from experiment where the tracer was planted at a 40cm depth just south of station W6. Tracer concentrations are given in (moles/kg-soil), and total head in (cm-water). Profile view taken along axis AA' shown in the plan view.

TABLE 2

Summary of Tracer Recovery and Anisotropy Esimates from Tracer Experiments.

Plume ID (Station Number)	Sampling Date	% Tracer Recovered	Ground Surface Slope (β)	qs/qn	Anisotropy
W6S	9/25/88	92	6^o	1.0	9.5
W3S	9/25/88	110	15^o	4.5	16.9
W3S	10/16/88	140	15^o	3.0	11.3
W2S	10/16/88	100	8^o	0.7	5.1

parallel and normal to the land surface which slopes at an angle of β. The situation is depicted schematically in Figure 10. If a wetting front advances perpendicular to the land surface, and if the soil pressure head (ψ) is perfectly correlated in the direction parallel to the slope, s, $\left(\frac{\partial \psi}{\partial s} = 0\right)$, then one can compute the soil–water fluxes as:

$$q_s = K_s sin\beta \tag{2}$$

$$q_n = K_n \left(\frac{\partial \psi}{\partial n} + cos\beta\right) \tag{3}$$

where q_s is the soil–water flux in the direction parallel to the slope, q_n is the soil–water flux in the direction, n, normal to the slope, and K_i is the hydraulic conductivity in the i direction. If one assumes s and n represent the principal directions, then one can use equations (2) and (3) coupled with the measured hydraulic heads to compute the effective anisotropy expressed as K_s/K_n. Assuming that the vector between the original solute source location and the center of mass of the solute plume at the time of sampling is indicative of the soil water flow paths, one can use the plumes to estimate q_s/q_n. Depending on the plume selected, q_s/q_n varies between 0.7 and 4.5. Owing to the fairly uniform, near unitary downward hydraulic gradient observed below a 30 cm depth, the estimated effective anisotropy ranges from 5.1 to 24.9 at a fairly uniform (in both space and time) pressure head ranging between 40 and 60 cm

of water. The average effective anisotropy for all of the experiments is 11.4. Table 2 presents the tracer data used to estimate effective anisotropy. This table of anisotropy estimates is broken down according to tracer source depth (recalling that the 40 cm depth source experiments were conducted south of the transect, and the 10 cm source experiments were conducted north of the instrumentation transect).

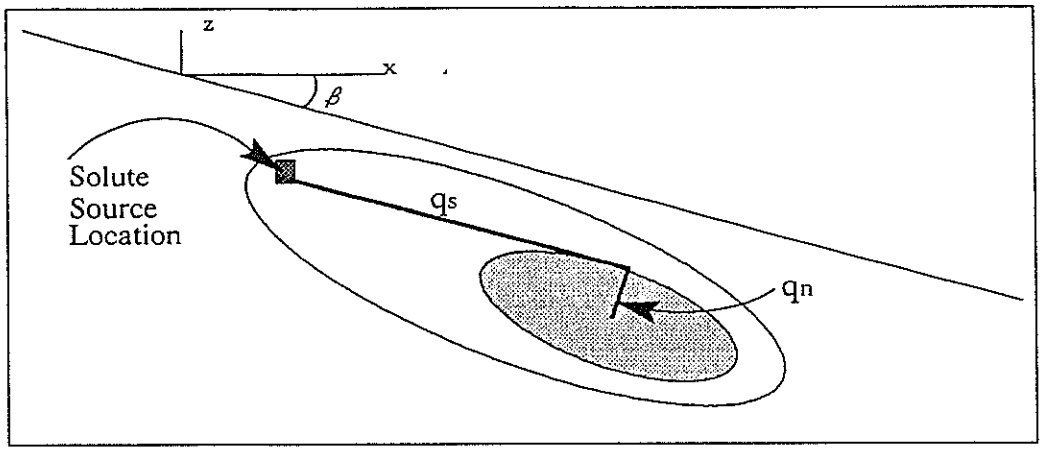

Figure 10. Schematic diagram showing how macroscopic anisotropy is estimated using plume geometries observed in field tracer experiments.

For comparison to the anisotropy estimated obtained from tracer plume geometry, two different procedures were employed to estimate the effective anisotropy at complete saturation. Both approaches indicated that the tracer site soils have an anisotropy ratio of about 1.5:1 under saturated conditions.

Soil Characterization

As mentioned in the Site Description section, a trench excavated at the site revealed no obvious fine–grained horizons of lower permeability. However, since visual appearances may be misleading, we performed a detailed grainsize analysis at several locations. A plot of the D_{10} and the D_{60} grain sizes versus depth for one such location (station W1) is presented in Figure 11.

Two different methods were employed to estimate the anisotropy ratio of the soils at complete saturation. The first method consisted of obtaining large scale (7.6 cm diameter x 25 cm length) samples oriented both parallel and perpendicular to the dune stratifications and performing constant head permeameter experiments on these samples. The anisotropy ratio was computed simply by dividing the measured saturated conductivity of the samples oriented parallel to the bedding by that of the samples oriented perpendicular to the bedding. This method predicted an anisotropy ratio at saturation equal to 1.54. Table 3 presents the field data obtained from these large scale permeameters. The other method used to estimate anisotropy at complete saturation is based on the fact that the equivalent saturated conductivity of a layered soil for flow in the direction parallel to stratification can be calculated by simply determining the arithmetic mean of the individual conductivities for each layer, whereas the equivalent effective conductivity in the

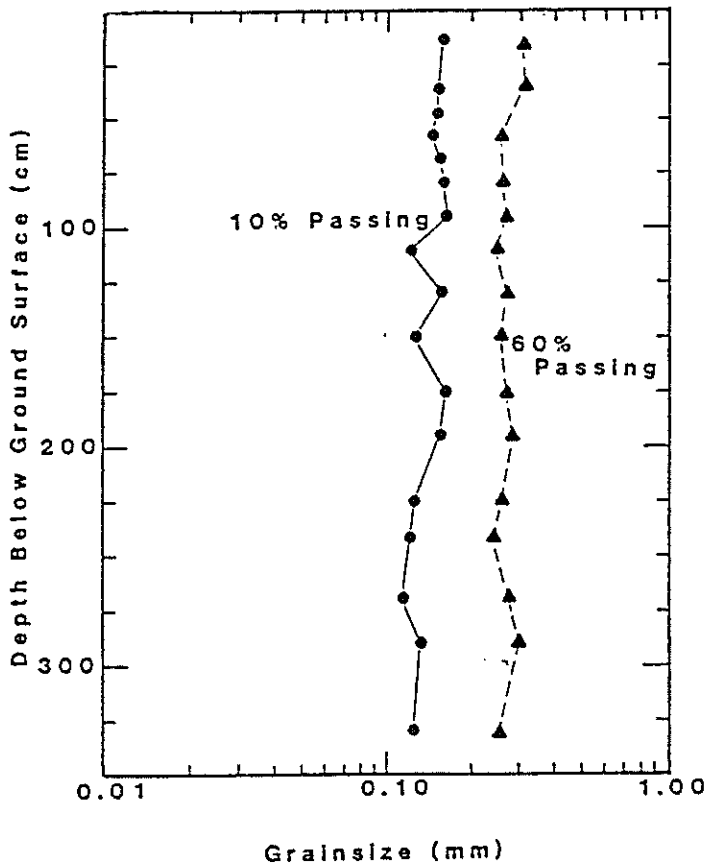

Figure 11. Typical plot of grainsize (D_{60} and D_{10}) versus depth profile from dune site.

TABLE 3

Summary of Results from Large Scale Saturated Permeameter Analyses.

Sample ID	Orientation	Ksat (cm/sec)
W2V@30	Perpendicular	1.40×10^{-2}
W2V@75	Perpendicular	1.64×10^{-2}
W3V@30	Perpendicular	1.45×10^{-2}
W3V@75	Perpendicular	1.44×10^{-2}
W3V@60	Perpendicular	1.35×10^{-2}
W3V@75	Perpendicular	2.04×10^{-2}
W3V2@60	Perpendicular	1.49×10^{-2}
W3V2@75	Perpendicular	1.62×10^{-2}
W2W@75	Parallel	1.37×10^{-2}
W3W@30	Parallel	2.19×10^{-2}
W3W@30	Parallel	2.66×10^{-2}
W3W2@30	Parallel	2.28×10^{-2}
W3W4@30	Parallel	2.28×10^{-2}
W2S@30	Parallel	2.23×10^{-2}
W3S@75	Parallel	2.26×10^{-2}
W3S2@30	Parallel	1.92×10^{-2}
W3S4@30	Parallel	1.78×10^{-2}

direction perpendicular to stratification can be calculated as the harmonic mean. If the number of samples is large enough, one can estimate the probability density distribution of the saturated conductivity, $f(k_s)$. Then the arithmetic mean can be defined as

$$K_A = \int_{k_1}^{k_u} k_s f(k_s)\, dk_s \tag{4}$$

the harmonic mean can be defined as

$$K_H = \left(\int_{k_1}^{k_u} \frac{1}{k_s} f(k_s)\, dk_s \right)^{-1} \tag{5}$$

with k_l the lower limit and k_u the upper limit of conductivity (Mualem, 1984), and the anisotropy ratio can be defined as K_A/K_H. To apply this approach constant head permeameter experiments were conducted on 82 samples of the dune sand. Then both the actual conductivities and the natural log of the conductivities were plotted on Gaussian probability paper. These plots indicated that the random conductivity field is best described by a lognormal distribution. The mean and variance estimates of the $ln(k_s)$ field are 3.53 and 0.82, respectively. Substituting this lognormal distribution into equations (4) and (5), one obtains an anisotropy ratio at full saturation of 1.51.

Clearly, this experimental work indicates that the Sevilleta dune sands are much (an order of magnitude) more anisotropic under *in situ* unsaturated conditions than they are in a saturated state. This result strongly supports the assertion of Yeh et al. (1985b), Mantoglou and Gelhar (1987c), and others (Mualem, 1984; Bear et al., 1987) that for variably saturated soils the effective anisotropy will vary significantly as the hydraulic state of the media changes. Two other notable large-scale field experiments designed to test the stochastic theories of flow and transport in unsaturated soils have recently been undertaken. The experimental approaches are much different than those employed herein,

and they are described in papers by Stephens et al. (1988) and Wierenga (1988).

Comparison of Field Estimated Anisotropy to Theoretical Estimators

For comparison to the macroscopic anisotropies estimated in the field tracer experiments, it is desirable to calculate anisotropy using independently derived estimators. For moisture contents less than 100%, three approaches are used to estimate anisotropy. The first approach, that of Mualem (1984), employs the definition of effective anisotropy for layered soils as being equal to the ratio of the arithmetic media conductivity to the harmonic mean. In the second approach, a Monte Carlo procedure is used to estimate the effective anisotropy of layered soils. And the third approach will make use of the stochastic result of Yeh et al. (1985b).

To use Mualem's (1984) method, we begin by assuming that the unsaturated conductivity of each stratification in a layered soil can be characterized as a function of pressure head, ψ, and saturated conductivity, k_s, and that k_s is a random variable. Depending on the relative conductivity function selected, there may be a number of other parameters, referred to here as α_i for generality, which affect the character of the unsaturated conductivity function:

$$K(\psi) = g(\psi, k_s, \alpha_i) \tag{6}$$

It can be shown that at complete saturation, the equivalent saturated conductivity of a layered soil for flow in the direction parallel to stratification can be calculated by simply determining the layer thickness weighted arithmetic mean of the individual conductivities for each layer; whereas the equivalent effective conductivity in the direction perpendicular to stratification can be calculated as the harmonic mean. If the number of samples

is large enough, one can estimate the probability density distribution of the saturated conductivity, $f(k_s)$. Then the arithmetic mean can be defined as

$$K_A = \int_{k_l}^{k_u} k_s f(k_s) dk_s \tag{7}$$

and the harmonic mean can be defined as

$$K_H = \left(\int_{k_l}^{k_u} \frac{1}{k_s} f(k_s) dk_s \right)^{-1} \tag{8}$$

with k_l the lower limit and k_u the upper limit of conductivity, and the anisotropy ratio can be defined as K_A/K_H. In his study Mualem (1984) extends this approach into the unsaturated domain by replacing the k_s in the integrand of the above expressions with $g(\psi, k_s, \alpha_i)$. Substituting the relative conductivity function (eqn. 1) into equations (2) and (3) and employing the definition of the anisotropy ratio as K_A/K_H, one can then derive the following expression for anisotropy as a function of pressure head,

$$U(\psi) = \left[\int_{k_1}^{ku} g(\psi, k_s, \alpha_i) f(k_s) dk_s \right] \cdot \left[\int_{k_1}^{k_u} \frac{f(k_s)}{g(\psi, k_s, \alpha_i)} dk_s \right] \tag{9}$$

To apply this approach constant head permeameter experiments were conducted on 82 samples of the dune sand. Then both the actual conductivities and the natural log of the conductivities were plotted on Gaussian probability paper. These plots indicated that the random conductivity field is best described by a lognormal distribution. The mean and variance estimates of the $ln(k_s)$ field are -3.53 and 0.82 (with k_s in $cm/sec.$), respectively. One can account for random α by also making each α_i some function of k_s. To determine this anisotropy function for the sands from the field site, we numerically evaluated the above integral (eqn. 4) subject to the following conditions: (1) we utilized the probability density function of k_s which was discussed above; (2) we estimated the relative conductivity curve from moisture retention data for 13 soil samples using a non–linear least squares

fit to van Genuchten's (1980) model; (3) we fit this relative conductivity curve to an exponential conductivity function, $K(\psi) = k_s e^{-\alpha\psi}$; (4) we determined by linear regression functional relationships between k_s and α. We found the resulting anisotropy function to be quite sensitive to the choice of the $\alpha(k_s)$ functions. Figure 12 shows the $A(\psi)$ relationship obtained for power curve, semi–log, and linear fits for α versus k_s. Clearly, a linear relationship between α and k_s results in the highest predicted anisotropy, while a power functional relationship leads to the smallest anisotropy. In no case does Mualem's approach predict anisotropies at *in situ* tension heads (30 to 70 $cm - H_2O$) as large as those estimated from the tracer experiment data.

Mualem's (1984) approach is limited by the fact that the saturated hydraulic conductivity is the only truly random parameter considered (all the randomness in α occurs only through its one-to-one functional relationship to k_s) and no spatial correlation is considered. In addition, Mualem (1984) assumes that the harmonic mean is representative of the effective unsaturated conductivity of a layered soil for flow in the direction normal to bedding, as can be derived for the saturated flow case. A closer examination of the non-linear unsaturated flow equation indicates that this effective conductivity is not equal to the harmonic mean.

The following derivation demonstrates how the non-linearity of the unsaturated flow problem affects the effective conductivities of layered soils. For unsaturated conditions, the equivalent homogeneous conductivity for flow parallel to the bedding of stratified media is the same as that obtained for saturated conditions:

$$K_{parallel}(\psi) = \frac{1}{D} \sum_{i=1}^{n} K_i(\psi) d_i \tag{10}$$

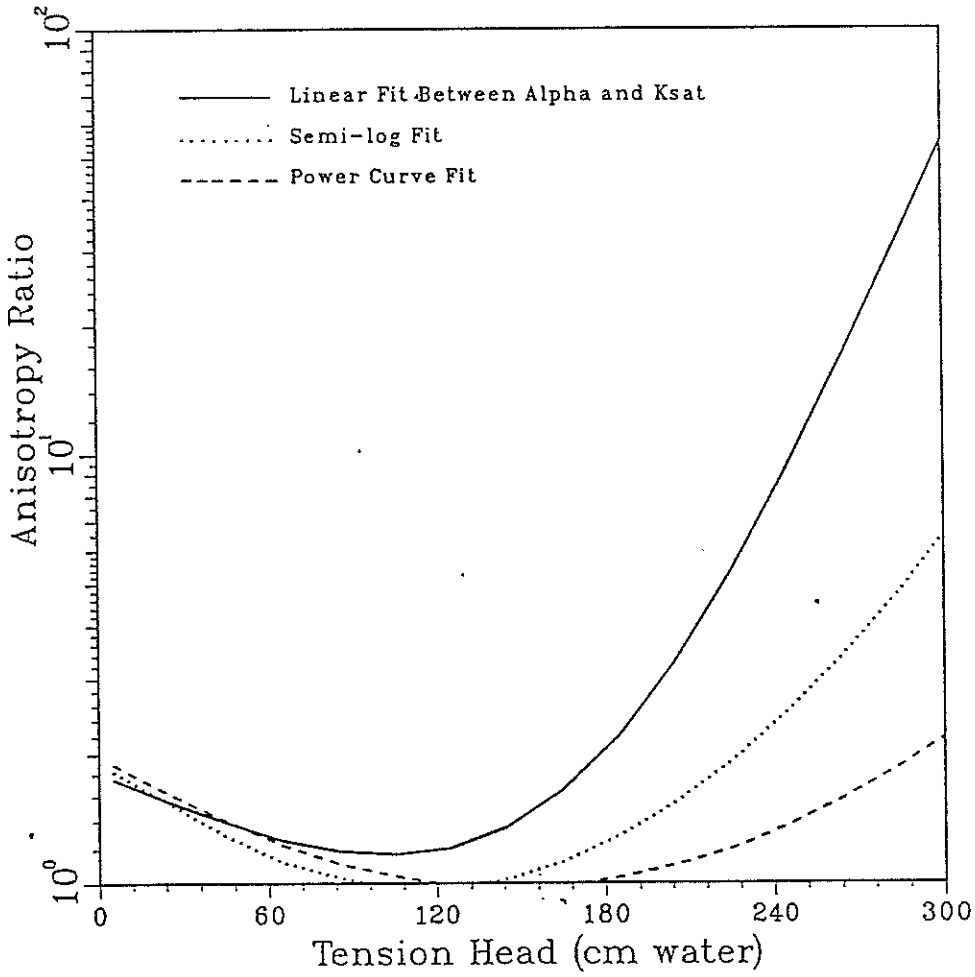

Fig. 12. Anisotropy as a function of pressure head for Sevilleta dune sands calculated by method of Mualem (1984) for three different functional relationships between α and k_s

where $K_i(\psi)$ and d_i are the unsaturated conductivity and thicknes of layer i, and D is the total system thickness. For unsaturated steady flow normal to bedding, the flow through each layer is equal the total flow through the system (by continuity):

$$q_i = K_i(\psi_i)\frac{\Delta h_i}{d_i} = q_{total} = K_{normal}(\Psi)\frac{\Delta h_{total}}{D} \tag{11}$$

where $K_{normal}(\Psi)$ is the equivalent homogeneous permeability for flow normal to bedding through a layered heterogeneous soil. Recalling that the total hydraulic head is the sum of the pressure head (ψ) and the elevation head, the first part of equation (6) can be re-written:

$$q_i = K_i(\psi_i)\frac{\Delta(\psi + z)_i}{d_i} \tag{12}$$

A brief inspection of equations (6) and (7) reveals that the non- linearity of the unsaturated flow problem complicates the determination of the effective equivalent permeability. To obtain a solution for the saturated case, one typically notes that Δh_{total} would equal the sum of all the Δh_i's and simply solves for $\Delta h_i = q_i d_i / k_{si}$. However, for unsaturated soils the conductivity is a non-linear function of ψ, which essentially precludes a compact analytical solution such as the harmonic mean derivation for saturated media which is presented in most groundwater text books (Freeze and Cherry, 1979). To obtain a solution for $K_{normal}(\Psi)$, one must select some form for the relative conductivity function for each layer, one must make some assumptions concerning how the capillary pressure head varies across each layer, ψ_i, and how to characterize the effective pressure head for the system, Ψ. Once all of these assumptions and decisions have been made, and after boundary pressure heads are specified and implemented into equation (7) for a media composed of n layers, one can obtain a system of n equations with n unknowns. One of the unknowns being q_{total}, the flux through the soil, and the other unknowns being the pressure heads

at the interface between each layer. Another possible solution technique would be to specify a flux through the system and then determine the pressure head for each layer by iteratively applying the analytical solution developed by Yeh (1988). As a fairly simple and straight-forward solution to this problem, we implemented a Monte Carlo approach.

The Monte Carlo approach employed can be briefly summarized as follows: (1) a two layer system was examined, the unsaturated hydraulic conductivity function for each layer was characterized by the exponential function $K(\psi) = k_s e^{-\alpha\psi}$; (2) saturated hydraulic conductivity values for each layer were randomly generated from the lognormal distribution estimated from the permeameter measurements of the Sevilleta sands described previously; (3) a unitary (gravity driven) hydraulic gradient was specified across the system (the pressure heads at the inlet and at the outlet were specified to be equal); (4) the effective permeability for flow parallel to stratifications was calculated as the arithmetic mean; (5) for flow perpendicular to bedding, a solution for the effective conductivity was obtained under the assumption that pressure head varied linearly across each layer and the mid-layer pressure head was used in the relative permeability function. Anisotropy was then calculated as the ratio of the effective conductivity for flow parallel to strata to the effective conductivity for flow normal to strata. Figure 13 presents the results obtained from 1000 Monte Carlo simulations. Also shown in the figure is the anisotropy predicted by Mualem's (1984) approach for a linear relationship between α and k_s. All of these estimators predict a minimum anisotropy at tension heads in the vicinity of those observed at the field site (30 to 70 $cm - H_2O$). At tension heads between 60 and 160 cm, the Monte Carlo approach predicted higher anisotropy ratios than those determined using Mualem's approach; however, they were still smaller than those estimated from the

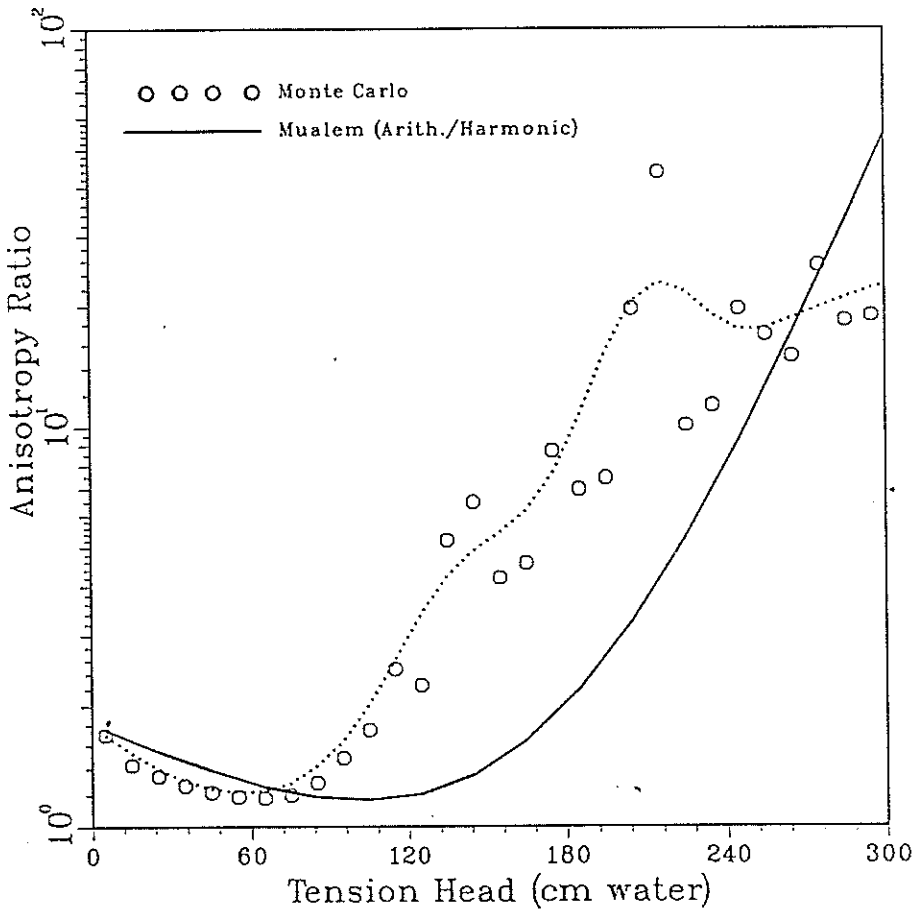

Fig. 13. Anisotropy as a function of pressure head obtained by Monte Carlo simulation of 1D flow through 2 layer system. For comparison the Mualem method result (for linear $\alpha(k_s)$ function) is plotted. Dotted line shows a smoothed representation of the Monte Carlo results.

tracer experiments described earlier.

As discussed in the Introduction, Yet et al. (1985a,b) and Mantoglou and Gelhar (1987a,b,c) used spectral stochastic techniques to analyze unsaturated flow in porous media. These studies directly tackle the two shortcomings of Mualem's (1983) study. Yeh et al. focus on the steady flow problem, while Mantoglou and Gelhar address the more general transient flow problem. Henceforth we will refer to the work by Yeh et al. (1985a,b,c) as "Yeh" and the papers by Mantoglou and Gelhar (1987a,b,c) as "MG," and in general references to both studies we will simply refer to them as "the stochastic researchers." Below we will briefly re-cap the approach they use to investigate this problem, and we will present some important results with respect to anisotropy of unsaturated soils. In their studies, the stochastic researchers used an exponential conductivity function:

$$K(\psi) = k_s e^{-\alpha\psi} \tag{13}$$

where K_s and α both can be considered random fields. In their analysis of transient flow, MG further assume that the moisture content-pressure head relationship, typically expressed in the flow equation as the specific moisture capacity, $C(\psi) = \partial\theta/\partial\psi$, can also be considered a random field. These random parameters can be utilized in conjunction with mass balance principles and Darcy's law to obtain the standard variably saturated flow equation (Richards equation):

$$\frac{\partial}{\partial x_i}\left[K_{ij}(\psi)\frac{\partial(\psi+z)}{\partial x_i}\right] = C(\psi)\frac{\partial\psi}{\partial t} = \frac{\partial\theta}{\partial t} \tag{14}$$

where x_i represent the orthogonal components of a three dimensional cartesian coordinate system (with z being positive in the vertical downward, gravity, direction) and the Einstein summation convention is used. As previously noted, the soil hydraulic properties

are considered random fields; the stochastic researchers thence assume that these local properties can be expressed as a mean value plus a perturbation:

$$ln(k_s) = F + f \quad , \qquad \alpha = A + a \quad , \qquad C = \Gamma + g \tag{15}$$

where F, A, and Γ are large-scale mean components of the random properties, while f, a, and g represent small-scale, local perturbations of $ln(k_s)$, α, and C, respectively. The stochastic theory which they develop assumes that F, A, and Γ are essentially constant at the scale of the flow domain under consideration, while the local variations occur over a scale much smaller than the spatial domain considered. Given that the soil hydraulic properties are actually random processes, then substitution of these random fields into the local flow equation (eqn. 9) as inputs leads to the conclusion that the pressure head also should be considered to be a random output of the system, and can therefore be expressed:

$$\psi = H + h \tag{16}$$

where H represents the large-scale mean value of the pressure head and h is the local fluctuation. Substituting the random processes expressed in equations (15) and (16) into the flow equation yields a pde with stochastic parameters $ln(k_s)$, α, and C, and stochastic output ψ.

Taking expected values of this resulting stochastic pde yields the following large-scale mean flow equation:

$$\frac{\partial}{\partial x_i}\left[\hat{K}_{ij}\frac{\partial(H+z)}{\partial x_i}\right] = \hat{C}\frac{\partial H}{\partial t} = \frac{\partial \Theta}{\partial t} \tag{17}$$

It is interesting to note that the large-scale equation is of the same form as the standard Richards equation (eqn. 14) parameterized with the effective properties $\hat{K}_{ij}$, $\hat{C}$, and the

effective state parameter Θ. In their analyses, the stochastic researchers show that these effective parameters depend not only on the mean hydraulic properties F, A, and Γ, but they also depend on the stochastic properties of the soil property fluctuations (i.e., variances and correlation lengths of f, a, and g) and the mean flow conditions (i.e., H, $\partial H/\partial t$, and $\partial H/\partial x_i$).

To determine the effective properties, the stochastic researchers subtract the mean flow equation from the general stochastic pde to obtain a mean-zero perturbation pde. After neglecting higher-order products of perturbations, they solve the resulting perturbation equation by invoking the Spectral Representation Theorem (Lumley and Panofsky, 1968). In essence, the Spectral Representation Theorem (SRT) allows one to uniquely represent second-order stationary (constant variance and covariance function) random fields by inverse Fourier transforms of complex stochastic processes. Thus the perturbation pde is transformed into the frequency domain, wherein the solution is obtained. Other properties of the SRT permit one to find relationships between the stochastic properties of the parameters in the spatial domain (first and second moments, as well as spatial correlation lengths) and their spectral densities in the frequency domain. Through this procedure they find relationships between the stochastic properties of the inputs ($ln(k_s)$, C, and α fields) and the stochastic properties of the output (first and second moments, and correlation length of the ψ field). Among the interesting results which they derive is the fact that the variance of the capillary tension increases significantly as the mean capillary tension increases. This result is supported by the field data of Yeh et al. (1986). In another study, Monte Carlo analysis of one-dimensional unsaturated flow by Yeh (1988) provides strong support for the spectral stochastic results obtained for one-dimensional

flow. Another very important conclusion of the stochastic researchers is the prediction of a state-dependent anisotropic behavior of the large-scale effective conductivity, $\hat{K}_{ij}$. For steady flow conditions, Yeh derived the following expression for effective anisotropy for unsaturated, layered soils with a mean hydraulic gradient directed in the vertical downward direction with a magnitude J_z, and uncorrelated $ln(k_s)$ and α fields:

$$U = \frac{\hat{K}_{11}}{\hat{K}_{22}} = exp\left[\frac{\sigma_f^2 + \sigma_\alpha^2 H^2}{1 + \lambda_1 A(2J_z - 1)cos\beta}\right] \tag{18}$$

where σ_f^2 is the variance of the log conductivity (lnk_s) random field, σ_α^2 is the variance of the slope of the lnK versus ψ relationship, A is the mean slope of lnK versus ψ, H is the mean value of ψ, λ_1 is the correlation length in the direction perpendicular to stratification, and β is the angle between the soil layer stratification and the horizontal. Yeh derived an expression of similar form for the case of perfectly correlated $ln(k_s)$ and α fields.

For comparison to the macroscopic anisotropies calculated from the field experiments, σ_f^2, σ_a^2, H, and A were estimated from field and laboratory data. Using equation (13) K_{11}/K_{22} was calculated for $\beta = 0^o$ and various values of λ_1. These results are plotted in Figure 14 along with the results using Mualem's approach for semi-log fit between α and k_s. As depicted in Figure 14, the stochastic approach predicts that anisotropy increases much more rapidly than Mualem's (1984) statistical method would predict, particularly for smaller correlation lengths (λ). The $\lambda_1 = 8\ cm$ curve predicts an anisotropy ratio at the *in situ* pressure heads which is close to that estimated from the field tracer data. It is quite obvious, however, that the anisotropy ratio calculated is extremely sensitive to the correlation length. A previous investigation into the spatial variability in saturated conductivity of the dune sands at the site suggests that correlation lengths are on the

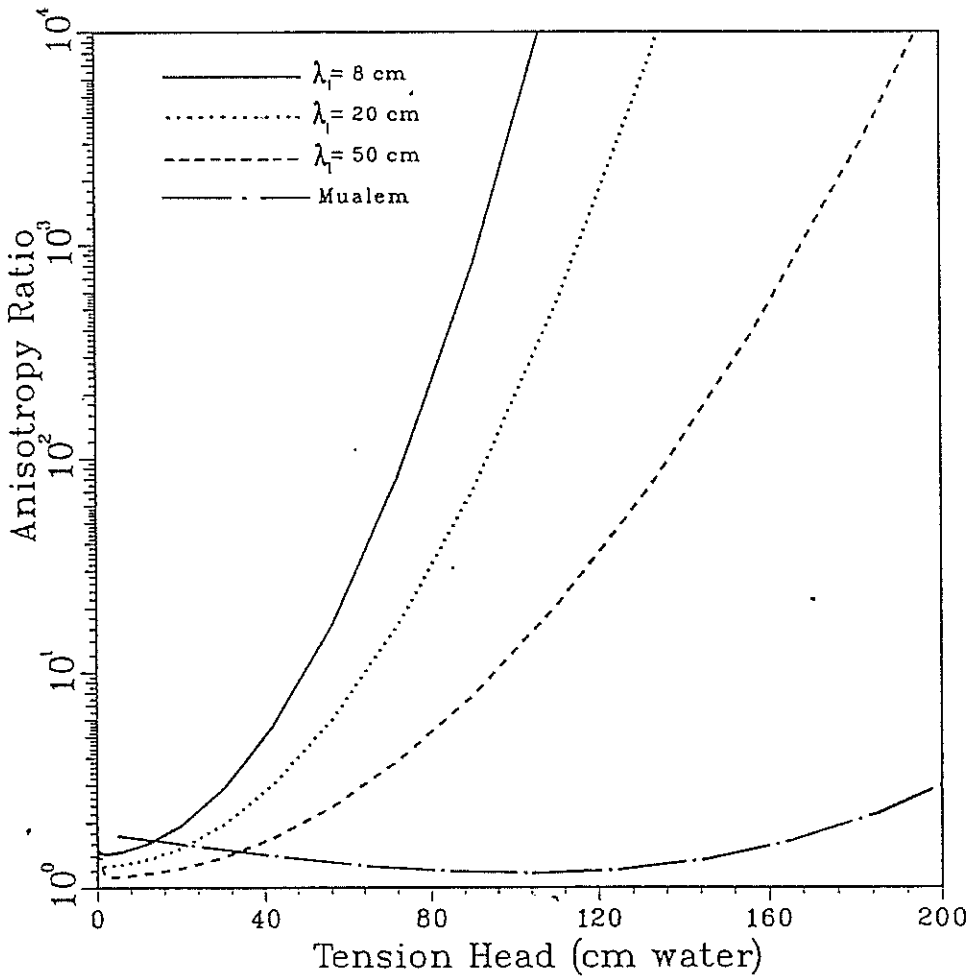

Fig. 14. Anisotropy as a function of pressure head calculated using stochastic estimator of Yeh et al. (1985b). Shown for comparison is result for Mualem's method with linear $\alpha(k_{sat})$ function.

order of the length of the sample rings (5 *cm*) or less.

DISCUSSION OF FIELD AND LABORATORY RESULTS

The depth versus concentration profile presented in Figure 3 demonstrates the large variability observed at most sampling locations, particularly those away from the solute source. These profiles were obtained downslope from the tracer source. In these experiments, the samples analyzed for tracer concentration ranged between 7 and 20 cm in length. In addition to true *in situ* concentration versus depth variability, there are some potential sources of error which may have contributed to the measured profile variations: (1) sample cross contamination due to sampling procedure, and (2) analytical errors in concentration determination (instrument drift, human error,...). One would intuitively think that sample cross contamination during sampling (sampling was performed by driving 1.5 cm diameter thin–walled tubes into the soils) would tend to cause a decrease in variability, due to smearing of the tracer along the sampling tube walls. With respect to sample analysis, although the human component of analytical errors is impossible to completely eliminate, the highly structured "cookbook" approach which was employed in the sample chemical analysis hopefully minimized human errors. Instrument drift also should be minimal due to the frequent recalibrations which were performed during sample analysis using bromide standard solutions. Assuming that errors are minimal in comparison to true *in situ* concentration profile variability, a couple important conclusions can be drawn. It is likely that if samples were obtained over smaller depth intervals, we would observe even greater concentration variability. This indicates that the vadose water tends to flow preferentially along discrete paths, even in the absence of pervasive large textural

variability. Similar microscale flow variability has been observed previously in transport through both saturated media (Ronen et al., 1987; Silliman and Simpson, 1987) and as well as in vertical infiltration into variably saturated soils (Kung, 1988; Hendrickx et al., 1988). This underlines the fact that classical deterministic analytical mathematical models (which are often employed to analyze observed tracer breakthroughs and predict flow and transport) inadequately describe the actual nature of fine–scale moisture movement in soil profiles. It is particularly significant in this case because one might *apriori* consider this sand dune to be composed of a very homogeneous material (see Figure 11) and thus deterministic analytical solutions developed for homogeneous media might apply. Such models predict very smooth flow and transport behavior, which is obviously not the case here. In many situations, however, one is interested primarily in the gross transport behavior of a solute; for such cases standard deterministic models may be adequate.

By applying a vertical averaging procedure to the measured bromide concentrations one can obtain the smooth solute plumes depicted in the profile views of Figures 4 through 9. The relatively high percent of bromide recovered (Table 2) suggests that the figures reasonably depict the actual plumes. The profile views demonstrate a large downslope horizontal component to the soil–water flow, while the relatively horizontal total head contours indicate a relatively steady, near vertical downward hydraulic gradient below a 30 cm depth. Above a 30 cm depth, however, gypsum block measurements indicate the soils often dried to tensions which exceeded the operation range of tensiometers, and thus it is likely that upward gradients existed at times. If upward hydraulic gradients did exist in the shallow soils, then the estimation procedure employed (see Figure 10 and equations 2 and 3) to obtain the anisotropies presented in Table 2 was based on flawed

assumptions *for the shallow source experiments.* The resultant plumes from the shallow source experiments would reflect complex flow behavior driven by highly variable hydraulic gradients. Therefore, we refrain from basing any conclusions concerning macroscopic anisotropy on results from the shallow source tracer experiments.

For the deep source experiments, the non–colinearity of the inferred flux and gradient vectors leads to the conclusion that the dune sand behaves as an anisotropic medium at the macroscopic scale. Simple darcian calculations applied to the plume geometries indicate that the degree of anisotropy ranges from 5.1 to 16.9. However, two independent, experimental procedures indicate that the anisotropy at complete saturation is about 1.5. Clearly the effective macroscopic anisotropy of the dune sand increases significantly upon desaturation. This field evidence substantially validates the qualitative result of Mualem (1984), Yeh et al. (1985b), Bear et al. (1987), and others who used analytical and experimental techniques to predict that anisotropy depends (at least in part) on the degree of saturation.

This result once again calls into question deterministic methods which are commonly employed in predictive numerical modeling of fluid movement in unsaturated media. Bear and Braester (1987) recommend that the typical approach of applying the same anisotropy ratio at all levels of saturation should not be used when modeling flow through *anisotropic* porous media. The grain size analyses (Figure 11) and the saturated conductivity measurements of the sands from our field site may lead one to assume that they closely approximate a homogeneous, isotropic medium. In this light, the results of our tracer experiments may lead one to question the prevalence (or, perhaps, even the existence)

of naturally deposited media which are hydraulically isotropic at all moisture contents. Therefore, following the lead of Bear and Braester (1987), we feel that the commonly used parameterization techniques for modeling variably saturated flow are inaccurate in most cases. Consequently, the question which remains is, what is the best estimator of the variable anisotropy function, and how might one account for a variable macroscopic anisotropy in a multidimensional flow code?

One possible method of calculating anisotropy is that proposed by Mualem (1984) (Equation 7). We applied this equation to hydraulic conductivity data for the dune sand, and the results are presented in Figure 12. Although anisotropy is predicted to increase greatly with decreasing pressure head, the anisotropy calculated by Mualem's method at *in situ* tensions (–30 to –70) is much less than that inferred from the tracer experiments at the field site. Although Mualem's (1984) method accounts for randomness in saturated conductivity, k_s, there are probably many other factors which influence hydraulic anisotropy. For example, to make the integrals (eq. 9) involved tractable, any variability in α can only occur through functional relationships to k_s. However, it is likely that α is better described by statistical cross–correlations to k_s, or perhaps α may vary statistically independently from k_s. In addition Mualem's approach fails to account for any spatial correlation structure in the parameters.

As shown previously, stochastic methods which account for spatial correlation structure can also be used to characterize hydraulic anisotropy in variably saturated, layered media (Yeh et al., 1985b). As depicted in Figure 14, the stochastic approach predicts that anisotropy increases much more rapidly than Mualem's (1984) statistical method would

predict, particularly for smaller correlation lenghs (λ). The $\lambda = 8$ cm curve predicts an anistropy ratio at the *in situ* pressure head ($-70 < \psi < -30$ cm) which is quite close to that estimated from the field tracer data. It is quite obvious, however, that the anistropy ratio calculated is extremely sensitive to the correlation length. A previous investigation into the spatial variability in saturated conductivity of the dune sands at the site (Leavitt, 1987) suggests that correlation lengths are on the order of the length of the sample rings (5 cm). Although the anisotropy predicted using the stochastic result of Yeh et al. (1985) with $\lambda = 8$ cm is within the range of values estimated from the tracer experiments, the difficulty of estimating some of the required input parameters based on field and laboratory testing leads to considerable uncertainty in applying this result (eq. 18) to the soils from our particular site.

Anisotropy of Texturally Homogeneous Media

Although the heterogeneity issues discussed above certainly must play a significant role in contributing to the lateral flow evidenced in the tracer tests, McCord and Stephens (1987) identified another potential contributing factor to macroscopic anisotropy which would occur even in a truly homogeneous profile. In a medium which is homogeneous in both texture and saturated hydraulic conductivity, a macroscopic anisotropid behavior can be induced by moisture-dependent heterogeneities in hydraulic conductivity. It is well known that fluid flow paths deflect as they pass from a medium of one conductivity into another of a different conductivity. Stochastic climatic inputs at the soil surface will lead to moisture content (and consequent hydraulic conductivity) heterogeneities in any soil profile, even one which may be considered homogeneous. The development of a

moist, high conductivity layer parallel to the ground surface of a hillslope would lead to horizontal downslope flow components if the hydraulic gradient field was oriented nearly vertical downwards.

Hysteresis in the soil moisture characteristics (moisture content-pressure head relationship) measured at the laboratory scale would tend to magnify the anisotropic behavior of homogeneous soils at the field scale. Hysteresis would prolong the effect of moisture-induced heterogeneities discussed above, due to the fact that this process slows the redistribution of infiltrated water. Simulation studies comparing one-dimensional infiltration and redistribution in hysteretic and non-hysteretic soils (Rubin, 1967; Hanks, et al, 1969) show that hysteretic media will develop a wetted zone which is less diffuse and has a higher peak water content than the wetted zone which would develop in comparable non-hysteretic media under the same boundary conditions. This higher peak water content will result in a larger contrast in hydraulic conductivity, and consequently a greater deflection of flow paths. Figure 15 show soil moisture characteristic data collected from 13 samples of Sevilleta dune sands. While the figure illustrates a bit of variability in the soil moisture characteristics, it also clearly shows that the field site materials are highly hysteretic.

The relative importance of textural heterogeneity and capillary hysteresis as causes of macroscopic anisotropy was determined through the diagnostic modeling investigation, which is discussed in the next section.

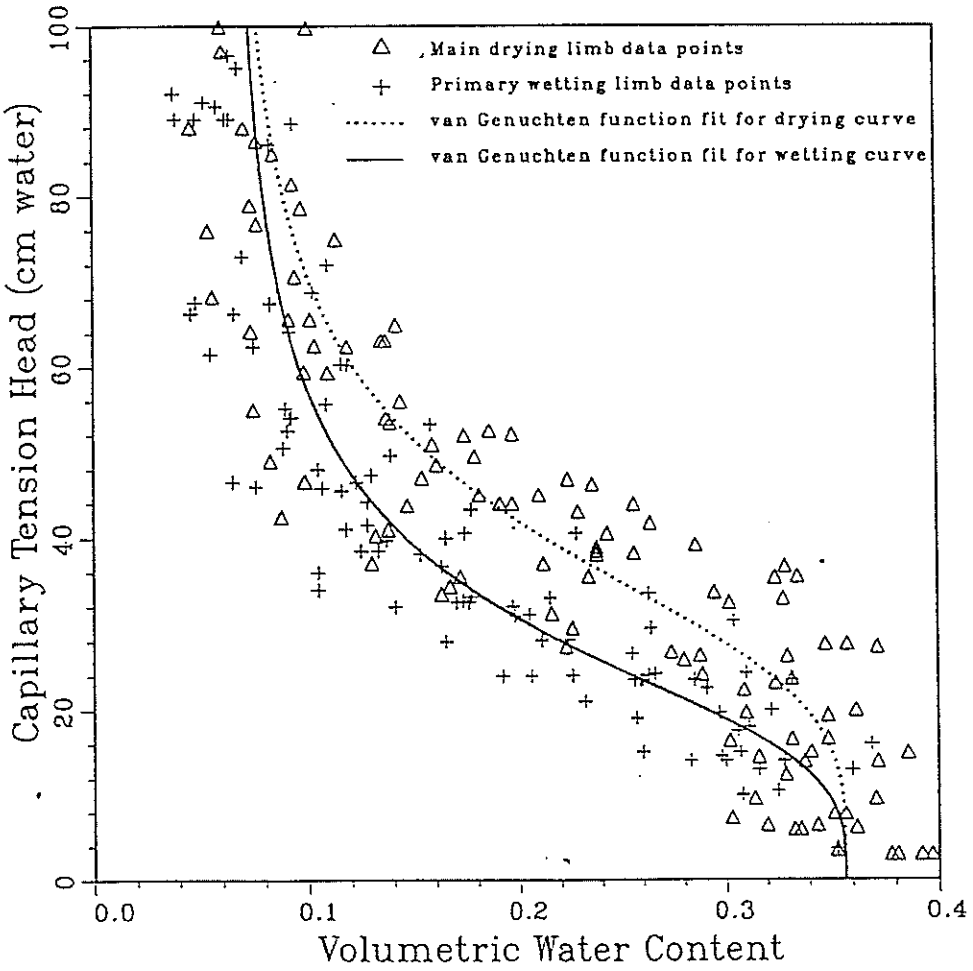

Fig. 15. Laboratory drying and wetting hanging column data from 13 samples plotted along with best fit curves for van Genuchten soil moisture characteristic function.

NUMERICAL MODELING

The field experiments indicate that the dune sands at the Sevilleta site behave as a highly anisotropic medium under unsaturated field conditions, yet laboratory and *in situ* permeameter experiments indicate that the Sevilleta sands are very nearly isotropic in their saturated state. Thus the anisotropy in hydraulic conductivity appears to be dependent on the hydraulic state of the medium, textural heterogeneity, and hysteresis-enhanced moisture-dependent variation in unsaturated hydraulic conductivity. In the following section, we attempt to determine the relative importance of textural heterogeneity and local hysteresis using a diagnostic numerical modeling approach. Based on the results of the diagnostic simulations, we performed a number of additional simulations to investigate the sensitivity of unsaturated flow and transport to precipitation intensity, geologic structure, and soil type.

First we cover the computer code which was used, citing its capabilities and indentifying its limitations. The code used in the following modeling exercise originally contained algorithms for neither hysteresis nor variable anisotropy caused by stochastic textural heterogeneity. Therefore, a good deal of the effort in this numerical modeling phase of the research was invested in implementing these two processes into the original code. Since variable anisotropy has received only minor recognition in journal publications to date, much of the discussion in the following section addresses the code alteration procedures with respect to variable, state-dependent anisotropy. After discussing the code modification procedures and validations, the conceptual model of the problem studied is defined. Next the design of the mesh used to discretize the spatial domain is covered. And finally,

we present both the diagnostic and sensitivity modeling results.

Traditional Mathematical Modeling Approach

In predictive modeling of flow through variably saturated media, one typically solves the Richards equation (see equation 9). The model which we used (VAM2D, will be discussed in more detail below) considers the case of two-dimensional flow. For two-dimensional flow with the (x, z) cartesian computational coordinates aligned with the principal directions of anisotropy and horizontally stratified media, equation (14) can be re-written:

$$\frac{\partial}{\partial x}\left[K_{xx}(\psi)\frac{\partial \psi}{\partial x}\right] + \frac{\partial}{\partial z}\left[K_{zz}(\psi)\frac{\partial}{\partial z}(\psi + z)\right] = C(\psi)\frac{\partial \psi}{\partial t} \tag{19}$$

Usually the directional unsaturated conductivities in (19) are considered as the product of the directional conductivity at saturation, k_{ii}, and a relative conductivity function, $K_r(\psi)$. The same relative conductivity is assumed to apply in all directions resulting in the following formulation:

$$\frac{\partial}{\partial x}\left[k_{xx}K_r(\psi)\frac{\partial \psi}{\partial x}\right] + \frac{\partial}{\partial z}\left[k_{zz}K_r(\psi)\frac{\partial}{\partial z}(\psi + z)\right] = C(\psi)\frac{\partial \psi}{\partial t} \tag{20}$$

We see that this traditional formulation leads to an anisotropy ratio (k_{xx}/k_{zz}) which is constant at all saturations.

We solved (20) and its later modifications using VAM2D, a finite element code which simulates flow and transport in two spatial dimensions. VAM2D was developed by Peter Huyakorn of HydroGeoLogic, Inc. A detailed coverage of the code's features can be found in the manual by Huyakorn et al. (1988), while Huyakorn et al. (1984) use the code to illustrate efficient techniques for solving the variably saturated flow equation. To implement hysteresis in VAM2D, we added an algorithm which accounts for linear scanning

curves (Hanks et al., 1969; Jaynes, 1984). This algorithm is not discussed further here. Allowance for variable state-dependent anisotropy was achieved by slightly modifying the mathematical formulation of the unsaturated flow equation and was implemented using the stochastic estimator (eqn. 18 in this paper) developed by Yeh et al. (1985b). Tracer movement was modeled using the transport portion of VAM2D.

Variable State–Dependent Anisotropy

In the paper by Bear et al. (1987), it is suggested that the orientation of the principal directions of permeability tensor may rotate as the saturation varies. Figure 5b in Bear et al. (1987) shows that the major axis at one level of saturation becomes the minor axis at another saturation. Although the field experiments of McCord et al. (1989) were not necessarily designed to be sensitive to such behavior, their results offer no indication of such a flip–flop in principal axes. For this reason, and since other theoretical analyses (Yeh et al., 1985b) do not predict such behavior, as well as for the sake of simplicity, the rotation of axes issue was not considered in developing the following formulation of a predictive mathematical model of unsaturated flow which considers variable anisotropy.

Recall that the stochastic researchers (Yeh et al., 1985a,b; Mantoglou and Gelhar, 1987a; see previous section) show that the effective parameters for their large-scale flow model depend on the mean soil hydraulic properties, on the stochastic measures of the soil property fluctuations (i.e., variances and correlation lengths of the lnk_s, and the $lnK - \psi$ and $\theta - \psi$ relationships), as well as on the mean flow conditions (i.e., H, $\partial H/\partial t$, and $\partial H/\partial x_i$). Given that this mean flow equation (eqn. 17) is of the same form as the standard variably saturated flow equation, it is reasonable to assume that numerical codes

developed to solve the standard equation could be used to solve this mean equation. To take such an approach, one need carefully consider the effective parameters which will be input to the model. As one of the goals of this study is to practically implement variable state-dependent anisotropy in a fashion which is consistent with the physical underpinnings of this phenomena as identified in theoretical analyses (Yeh et al., 1985b; Mantoglou and Gelhar, 1987a,b,c), we first address the practical issue of model implementation, then we will examine and select forms for the effective parameters which are appropriate for this study.

Implementing Variable Anisotropy. Rather than solving the variably saturated flow equation which is typically solved by numerical models (eqn. 20), we suggest solving the following equation:

$$\frac{\partial}{\partial x_i}\left[U_{ij}(\psi)k_{ij}K'_r(\psi)\frac{\partial(\psi+z)}{\partial x_j}\right] = C(\psi)\frac{\partial\psi}{\partial t} \tag{21}$$

where $U_{ij}(\psi)$ is the variable anisotropy function matrix, k_{ij} is the saturated conductivity tensor; and $K'_r(\psi)$ is a relative permeability function. For a two dimensional (x,z) system, if the computational coordinates coincide with the principal directions of anisotropy, let:

$$U_{ij}k_{ij}K'_r(\psi) = \begin{bmatrix}\sqrt{U(\psi)} & 0\\ 0 & 1/\sqrt{U(\psi)}\end{bmatrix}\begin{bmatrix}k_{xx}K_r(\psi) & 0\\ 0 & k_{zz}K_r(\psi)\end{bmatrix} = \begin{bmatrix}K_{xx}(\psi) & 0\\ 0 & K_{zz}(\psi)\end{bmatrix} \tag{22}$$

Therefore, referring to the standard pde solved (eqn. 14), $K_{xx}(\psi) = [U(\psi)]^{1/2}k_{xx}K_r(\psi)$ and $K_{zz}(\psi) = [U(\psi)]^{-1/2}k_{zz}K_r(\psi)$. This entire term in essence represents $\hat{K}$, the effective conductivity parameter for the large–scale mean flow equation developed by the stochastic researchers (Mantoglou and Gelhar; 1987a,c). Employing such a definition for $U_{ij}(\psi)$ prevents the hydraulic conductivity in the direction parallel to stratifications from taking on unreasonably large values under unsaturated conditions. The geometric mean conduc-

tivity for this formulation equals the geometric mean conductivity for the conventional formulation (eqn. 20).

This approach represents a "first cut" effort at implementing variable anisotropy in a numerical code, and can be achieved by making some relatively minor modifications to an existing unsaturated flow simulator. Our only modification was the inclusion of the $U_{ij}(\psi)$ as shown in equations (21) and (22). For simplicity we do not include the large-scale $\hat{C}$ parameter introduced by Mantoglou and Gelhar (1987b). Another approach would be to solve the standard form of the Richards equation parameterized by the directional unsaturated conductivity formulas developed by Yeh et al. (1985b, eqn. 33) or Mantoglou and Gelhar (1987c, eqns. 34-35), as discussed Polmann et al. (1988).

Selection of Variable Anisotropy Model. We chose to use a stochastic theory estimator for the function $A(\psi)$ because the theory compared favorably with the results of the field tracer experiments (McCord et al., 1989). To determine which variable anisotropy model was most appropriate for use in the flow simulator, a first-order sensitivity analysis was performed in conjunction with a quantitative examination of some trial simulation results. Yeh et al. (1985b) addressed the steady flow problem, while Mantoglou and Gelhar (1987c) show anisotropy (as well as mean moisture content) to be a function of the temporal mean pressure head gradient, $\partial H/\partial t$. In effect, this result suggests that layered heterogeneous soils exhibit a large-scale hysteretic behavior: the macroscopic hydraulic property function for a wetting layered soil profile differs from that for the same profile under drying conditions. In addition to general expressions for effective anisotropy as a function of H, $\partial H/\partial x_i$, and $\partial H/\partial t$, Mantoglou and Gelhar (1987c) developed asymptotic

solutions based on the value of the parameter which they term G:

$$G = e^{-F} e^{AH} \frac{\partial H}{\partial t} \tag{23}$$

The asymptotic expressions apply to the layered media dipping at an angle β, with the correlation length in the direction parallel to stratification, λ_1, much greater than the correlation length in the normal direction ($\lambda_1/\lambda_2 \rightarrow \infty$). For $G \rightarrow -\infty$, $K_{11} \approx K_{22}$; i.e., the media is effectively isotropic for rapidly drying conditions ($\partial H/\partial t \ll 0$). For $G \approx 0$ (essentially steady-state flow), for soils with uncorrelated α and f fields and with a mean hydraulic gradient directed in the vertical downward direction with a magnitude J_z, the macroscopic anisotropy could be calculated using the expression developed by Yeh et al. (1987b) and presented here as equation (18). For $G \rightarrow \infty$, rapid wetting, they found

$$U = \frac{\hat{K}_{11}}{\hat{K}_{22}} = exp\left[\frac{\sigma_f^2 + \sigma_\alpha^2 H^2}{\lambda_1 A(2J_z - 1)cos\beta}\right] \tag{24}$$

Equations (18) and (24) show that for a given mean pressure head H,. rapidly wetting soils ($\partial H/\partial t \gg 0$) are more highly anisotropic than soils under steady flow conditions.

To determine the importance of including the $\partial H/\partial t$ dependence (or "large-scale hysteresis" to apply the description of Mantoglou and Gelhar) in the variable anisotropy flow model, a trial simulation was performed. The results of this simulation were analyzed to determine the magnitude of $\partial H/\partial t$ at all nodes along a vertical transect from the ground surface to a two meter depth. The spatial domain and boundary/initial conditions modeled in the trial simulation are essentially the same as those subsequently used in the detailed modeling study. The scenario investigated consists of a three meter long hillslope composed of Sevilleta dune sands, initially in a relatively dry state (ψ_i = -80 cm water), subjected to an intense (5 cm/4 hr) precipitation event, followed by a period of

evaporation and redistribution. The temporal pressure head gradient (calculated using a backward difference) versus time at the ground surface from the trial simulation is plotted in Figure 16a. In addition, the factor G (eqn. 23) versus time is presented in Figure 16b. Both of these plots clearly indicate that the asymptotic limits ($G \rightarrow \pm\infty$, $\partial H/\partial t \ll 0$, and $dH/dt \gg 0$) are not approached at any time during the trial simulation, at any depth (even at the ground surface). One can note that G at the ground surface did approach a relatively large negative value at large time. This is primarily due to the fact that H, the mean capillary tension head, was getting quite large in response to the surface evaporative boundary condition. As H approaches larger and larger values, the unsaturated hydraulic conductivity decreases exponentially. Given the negligible conductivity at high H, it really doesn't matter what anisotropy value is used because the simulated fluid flux would be essentially zero within the time frame of event-based simulations. For long-term simulations net fluxes in dry materials may be appreciable, and thus one of the asymptotic anisotropy estimators for transient flow may be better. Since it appears that $\partial H/\partial t$ remains relatively small, it was concluded that the steady-state anisotropy expression put forth by Yeh et al. (1985b) would be a suitable estimator to use to numerically model flow at the Sevilleta field site.

When implementing this anisotropy estimator (eqn. 18) in a predictive model, one would need to measure or otherwise estimate the means, variances, and correlation lengths of the soil hydraulic properties. In a practical applied modeling sense, these stochastic parameters (means, variances, and correlation lengths) are simply material properties which the modeler would specify and which remain constant for the entire simulation. The dip angle of the soil stratifications, β, is another parameter which could be included

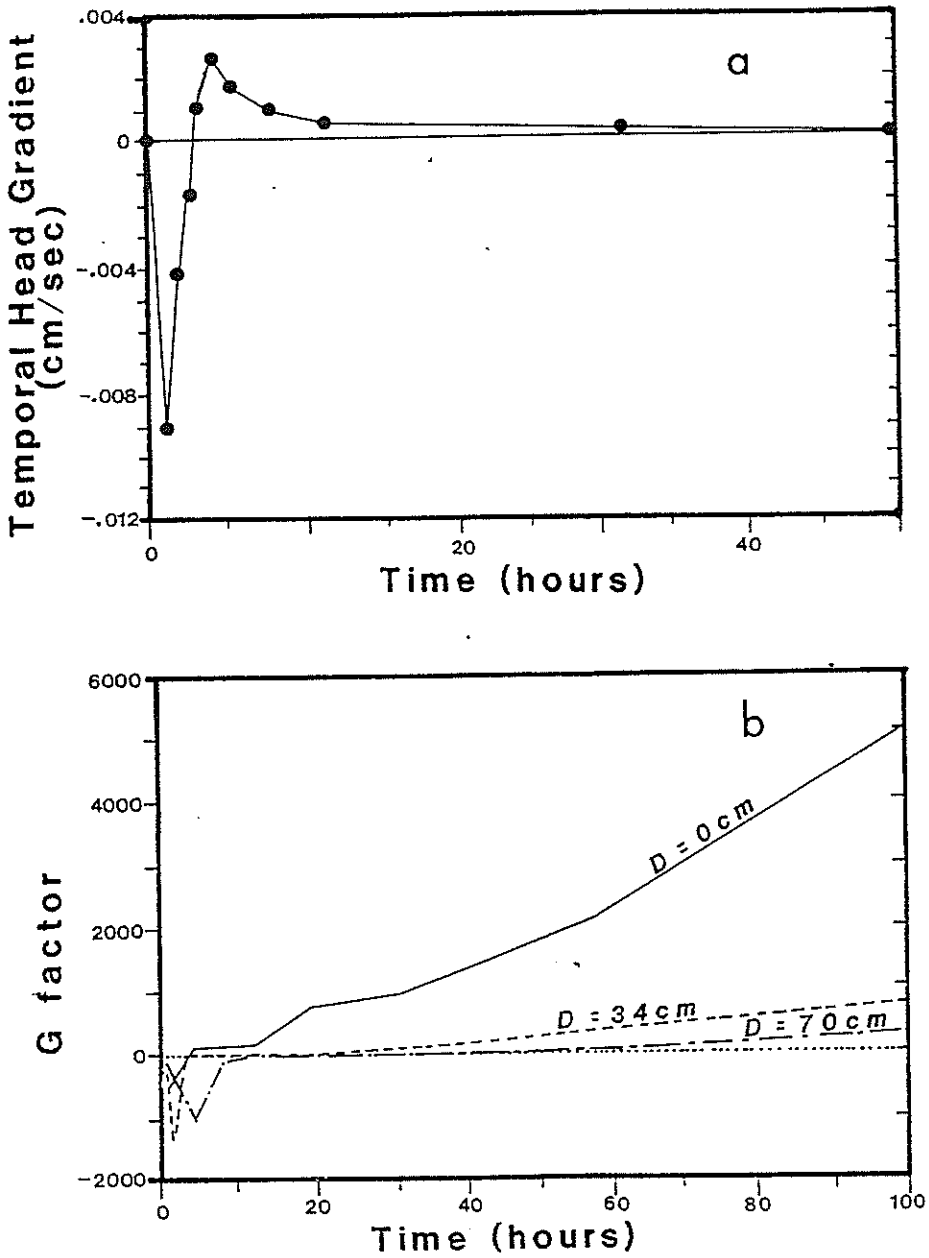

Fig. 16a. Temporal head gradient at the ground surface versus time from test simulation of flow in Sevilleta dune sand.

16b. G factor (see equation 18) versus time at various depths from test simulation of flow in Sevilleta dune sand.

as a constant material property. However, the two other important parameters, H (the mean pressure head) and J_z (the mean spatial head gradient in the vertical downward direction), are not material constants; they are additional non-linearities in the governing equation which have to be solved for within the existing non-linear iterative solution structure of the model. Having to calculate spatial head gradients, J_z, at every iteration could be excessively burdensome computationally. In an effort to include the simplest (for numerical solution purposes) yet most complete anisotropy model, a first-order sensitivity analysis (Dettinger and Wilson, 1981) was performed on equation (13) to investigate the importance of changes in the input parameters H, J_z, and β on model output. Results of the analysis are presented in Figures 17, 18, and 19. These figures graphically show first-order approximations of model sensitivity to changes in mean pressure head, mean head gradient in the vertical downward direction, and slope of media layers. In part A of each of these figures the sensitivities are presented in the form of coefficients of variation (standard deviation divided by the mean), while part B shows anisotropy versus each sensitivity independent variable. These results clearly show that the anisotropy model developed in the steady flow analysis (Yeh et al., 1985b) is most sensitive to changes in mean pressure head, is less sensitive to the mean head gradient, and is relatively insensitive to changes in dip angle of the porous media (particularly for $\beta < 30°$). Based on this first-order sensitivity analysis, we decided to make the anisotropy of each element a single-value function of the mean (centroidal) pressure head of that element.

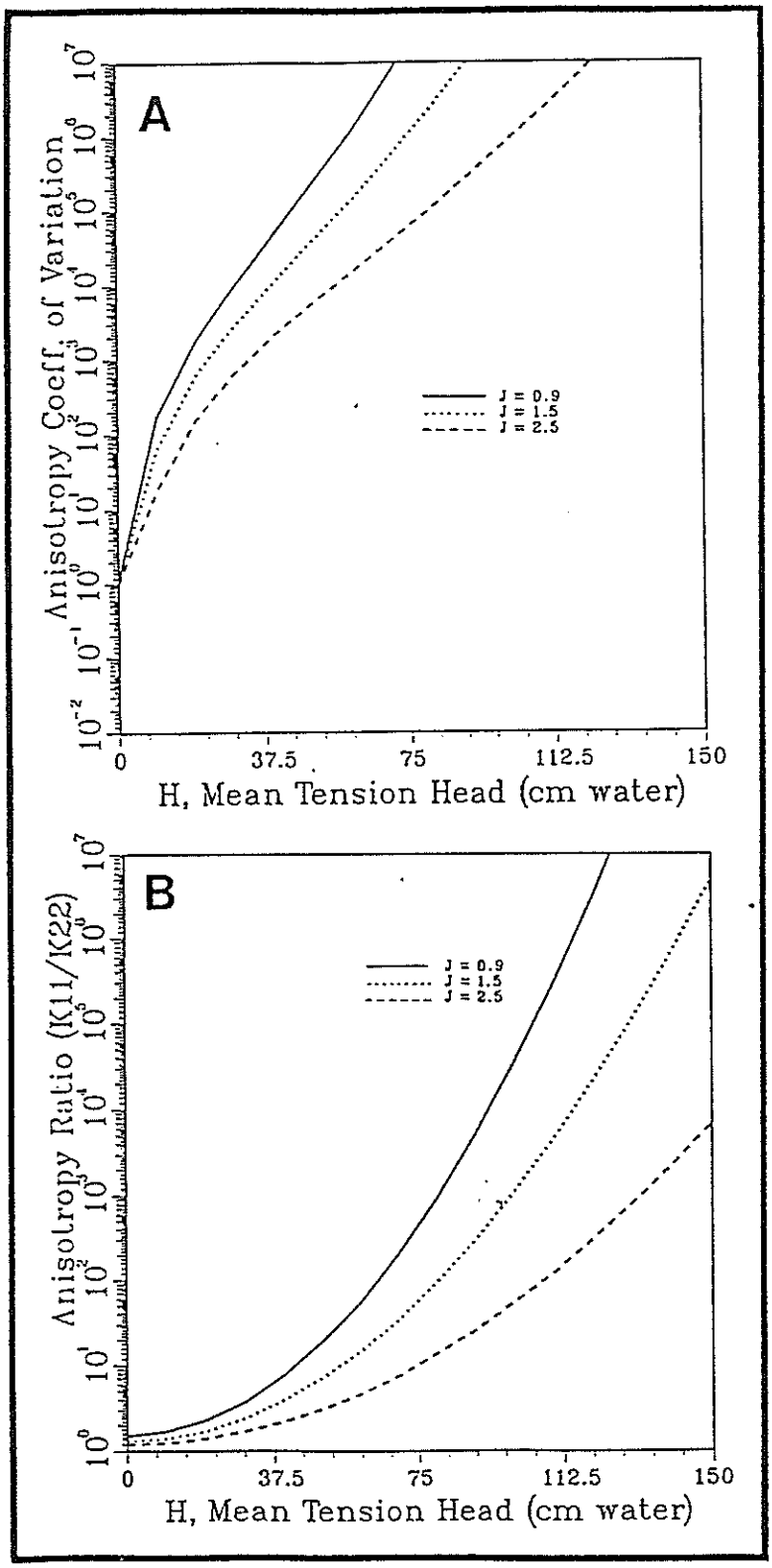

Fig. 17. Sensitivity of anisotropy to mean tension head for three different spatial magnitudes. A. Anisotropy coefficient of variation estimated by first order analysis; B. Anisotropy ratio as a function of mean tension head.

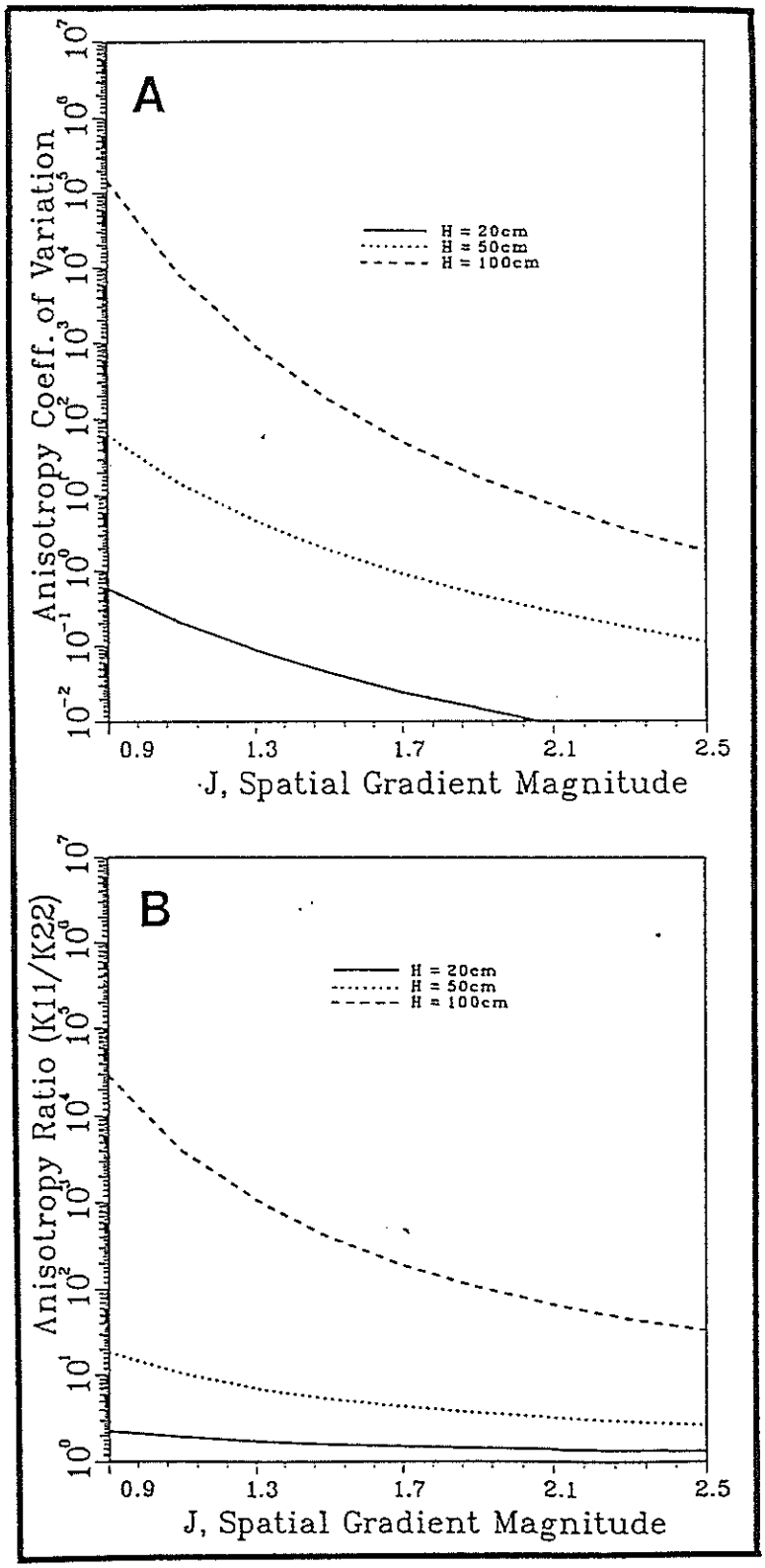

Fig. 18. Sensitivity of anisotropy to spatial gradient magnitude for three different values of mean tension head. A. Anisotropy coefficient of variation estimated by first order analysis; B. Anisotropy ratio as a function of gradient magnitude.

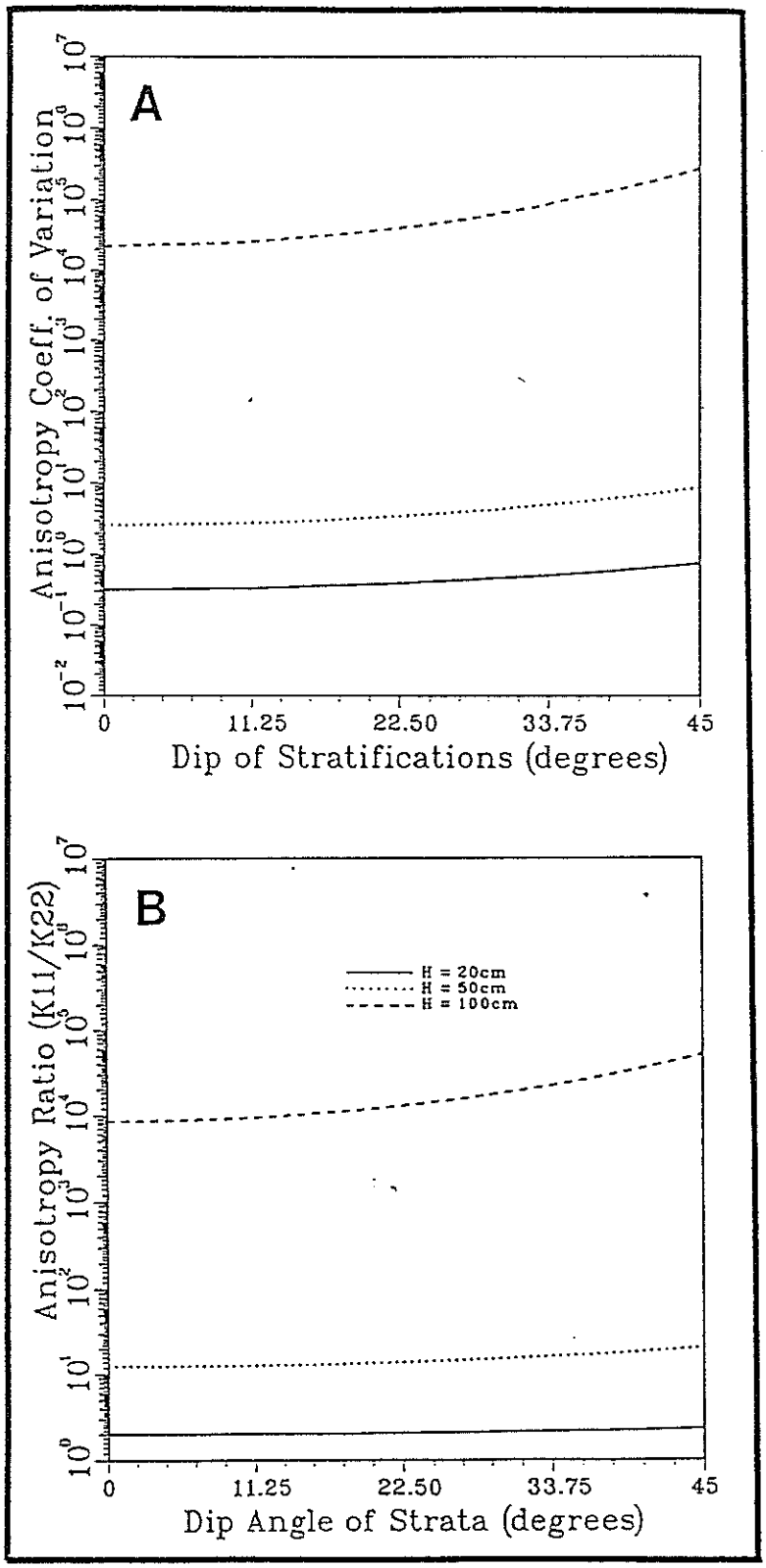

Fig. 19. Sensitivity of anisotropy to dip of media stratification plotted for three different values of mean tension head. A. Anisotropy coefficient of variation estimated by first order analysis; B. Anisotropy ratio as a function of dip.

MODEL APPLICATION

As mentioned previously, one of the primary objectives of this modeling exercise was determining the principal causes of the observed macroscopic anisotropic *behavior* of flow through the Sevilleta dune sands, and to provide some quantitative measure of the relative importance of the contributors to this behavior. The objective was not exactly simulating the flow fields and solute plumes observed. Therefore no effort was made to perform a calibration or inverse analysis to adjust model parameters to obtain a better fit between simulated and observed solute plumes. We felt that we lacked the data necessary to exactly model any particular event; just determining the true initial conditions for any such a modeling effort would be difficult (particularly considering the hysteretic nature of the field site soils). However, our data collection efforts certainly yielded sufficient information to characterize the statistics of the soil hydraulic properties of the Sevilleta dune sands and average *in situ* moisture conditions. To achieve our objective, we simulated a hypothetical hillslope composed of Sevilleta sands, with initial and boundary conditions which were representative of those observed at the field site, and which were easily verified to be internally consistent with the physics of the problem. We modeled the mean head distributions and the movement of the tracers.

Initially a series of simulations was performed to determine, or *diagnose*, the controlling processes at work at the Sevilleta site. To model the flow and transport behavior observed at the field site, we employed three independent approaches. In the first attempt, we solved the Richards equation neglecting hysteresis and employing the commonly used approach of considering hydraulic anisotropy to be constant (eqn. 15). For one set of sim-

ulations the soils were defined to be nearly isotropic (based on the saturated permeameter analysis); and for another set, based on the anisotropy estimates from the field tracer experiments, a constant anisotropy ratio of 10:1 was specified. In the second approach, the flow equation was once again solved considering a constant anisotropy ratio (1.5:1), but this time capillary hysteresis was accounted for. As discussed previously, consideration of hysteresis should enhance the development of moisture-dependent hydraulic conductivity variations in the porous media profile following infiltration and subsequent redistribution. These first two modeling approaches help us determine the magnitude of anisotropy enhancement by hysteresis. In the third approach hysteresis was neglected, but the variable anisotropy algorithm was included. Through this procedure, we attempted to identify the relative importance of the primary contributors to the lateral flow behavior observed in the field experiments.

Following the initial *diagnostic simulations* which were designed to determine the relative importance of hysteresis and variable anisotropy, another set of simulations was performed to investigate the impact of geology, topography, and precipitation characteristics on the unsaturated flow process. We henceforth refer to this series of model runs as the *sensitivity simulations*. Based on conclusions drawn from the diagnostic set of simulations, we specified variable anisotropy in all of the sensitivity simulations. One pair of runs looked at the effect of changing the orientation of the soil stratifications. In another simulation we decreased the precipitation intensity and increased the duration for comparison to the results for the high intensity storm modeled in the diagnostic set. The impact of gentler topography (less steep slopes) and a different soil type (clayey soil) were examined in the final two simulations.

Spatial Discretization and Mesh Design

In all simulations, the same finite element mesh (composed of rectangular elements) was used to discretize the spatial domain. By simply changing the Δx and Δy values in the finite element discretization, one could model a hillslope of any desired spatial dimension using the same mesh. Figure 20a schematically depicts the finite element mesh of the soil profile modeled. Areas in the figure identified as Soil I were specified as regions of horizontally stratified media, whereas Soil II represented media with a principal direction oriented parallel to the ground surface (since media stratifications were observed to roughly parallel the ground surface slope at the field site). Soil properties used (saturated conductivity, soil moisture characteristics, relative permeability) were those determined for the Sevilleta dune sands from the field site.

Two different spatial domains were modeled using the finite element discretization depicted in Figure 20a. Recognizing that large nodal spacing induces a significant amount of spurious numerical dispersion, McCord (1988) utilized a spatial moment analysis to determine objectively an appropriate nodal spacing to use in the tracer transport modeling. The first spatial moment of the modeled solute plume is indicative of transport instance, while the second spatial moment provides a measure of dispersion (Freyburg, 1986). The moment analysis procedure can be described as follows. Initially a simple two-dimensional flow and transport problem was defined: a spatial domain of a given size was subjected to a given set of boundary and initial conditions. In essence the problem investigated was unidirectional unsaturated flow through Sevilleta dune sands under an episodic flux boundary, with a point source of solute specified near the inlet boundary. Then, this problem was solved numerically several times, each time using a different spatial dis-

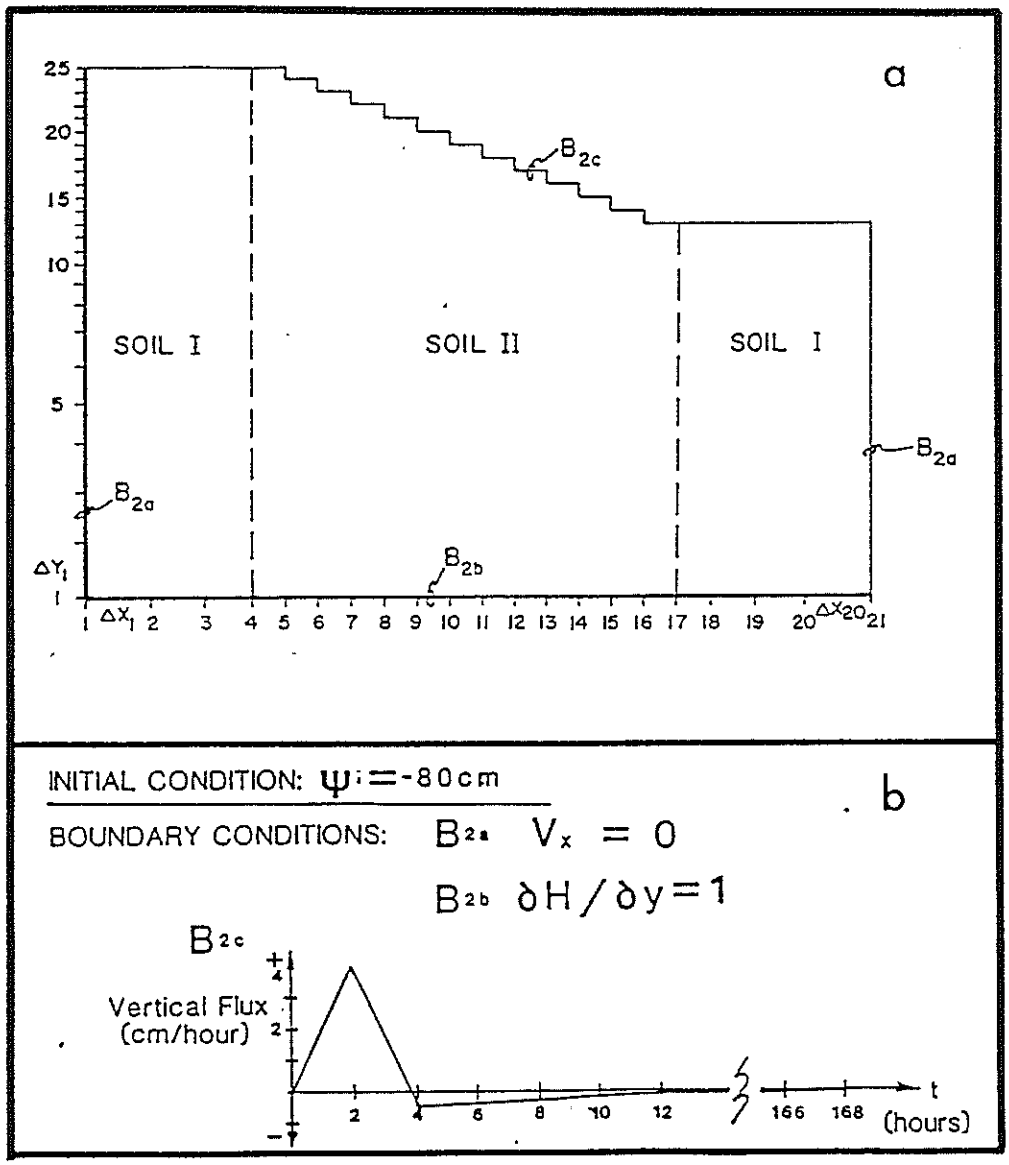

Fig. 20a. Spatial domain, boundary conditions, and porous media modeled in numerical simulations.

20b. Summary of initial and boundary conditions used in flow modeling. In the long duration, low intensity storm simulations, as well as those comparing the impact of soil lithology, the 5 cm of precipitation was applied over a 24 hour period.

cretization (starting with a very coarsely gridded mesh and successively fining up the grid for each subsequent simulation). Next, the plumes predicted by each of these simulations were subjected to a moment analysis. The spatial moments were estimated using a multi-dimensional trapezoidal numerical integration scheme (Burden and Faires, 1985). These results showed that numerical dispersion became apparent when nodal spacings were greater than about ten centimeters, and dominated with nodal spacings in excess of twelve centimeters. As expected, numerical dispersion was minimized at the smallest nodal spacing; however, even relatively coarse discretizations did a reasonable job at predicting transport distance. And finally, for the relatively fine grids, nearly doubling the computational effort did not buy much of a decrease in numerical dispersion.

Based on this spatial moment sensitivity analysis, we decided to perform most of the simulations using a relatively small nodal spacing, with Δx_4 through Δx_{17} (see Figure 20) specified the value of 12.5 cm, and Δy_8 through Δy_{25} assigned a value of 6.7 cm. The finite element mesh obtained from these assigned nodal spacings will henceforth be referred to as the *fine grid* or the *small domain*. The depth and breadth of the domain modeled by the fine grid are 270 cm and 300 cm, respectively. In three simulations we chose to employ larger nodal spacings. It has been proposed (McCord et al., 1988) that lateral flows induced by moisture-dependent permeability variations would be most pronounced when nodal separation distances are relatively small, so that moisture content (and consequent permeability) contrasts would not be attenuated significantly by the numerical averaging of element properties. To test this hypothesis a single simulation was performed with a fairly coarsely discretized spatial domain. Although this coarse grid allowed a significant amount of numerical dispersion to develop in the subsequent numerical solution of the

transport equation, the moment analysis (see the preceding paragraph) indicated that transport distance is reasonably modeled. In the coarse grid simulation we specified Δx_4 through Δx_{17} to be 50 cm, and Δy_8 through Δy_{25} to be 20 cm; and all other nodal spacings were scaled accordingly. The resulting mesh simulates a profile 800 cm in depth and 1200 cm in length. This mesh will henceforth be referred to alternatively as the *coarse grid* or the *large domain.* In the final series of simulations which examined the impact of gentler slope, as well as the simulations which examined the impact of soil lithologies, our primary interest was comparing gross flow behavior. Since the relatively large nodal spacings did a reasonable job at predicting transport distance, these final simulations also were performed using a coarse grid.

Boundary Conditions and Material Properties

For the flow problem, the boundary conditions applied to the system in all simulations were no flow on the sides, free drainage (specified unit gradient) at the base, and specified flux (precipitation/evaporation) at the ground surface. Figure 20b summarizes system initial and boundary conditions, including the temporal distribution of the surface flux rate (5cm/4hr, this roughly corresponds to a 10-year storm for the site). In the low intensity long duration storm simulation (as well as the gentle hillslope and clayey soil type simulations), 5 cm of precipitation was applied over a 24 hour period instead of the 4 hour period. For the hysteretic simulations as an additional initial condition, all nodes were specified to be drying along the main drying limb of the hysteretic $\theta - \psi$ curve. In essence, most of the simulations investigated the response of a hillslope profile (composed of Sevilleta dune sands) to a high intensity precipitation event followed by a period of evaporation and redistribution.

In the tracer transport simulations an antecedent solute concentration is specified to be zero everywhere except at one spot at a depth of about 30 cm near the top of the slope, which had a specified initial concentration equal to 1.0. Table 4 summarizes the porous media properties and grid conditions for the diagnostic simulations.

MODELING RESULTS

Modeling results are presented below. Salient features of these results are identified, but general discussion is withheld until the next section. It is important to note that in many of the forthcoming figures which depict the simulation results, only the small region of interest around the simulated solute plume is depicted even though a much larger domain was simulated (see Fig. 20a).

Diagnostic Simulations

The Role of Hysteresis. Figure 21 shows the velocity field, along with the water content and total head contours for a simulation (Case 2, see Table 4) with a fine grid and hysteretic isotropic media at a time near the end of the rainfall event. From this figure one may be able to infer a slight non-colinearity between the velocity vector and the gradient vector in places, even for this case of very small, constant anisotropy. This supports the assertion that moisture-dependent permeability variations can cause even homogeneous, locally isotropic soils to behave anisotropically when viewed at the field scale. Note that near the wetting front, where capillary gradients dominate, that velocity vectors have a strong component into (normal to) the hillslope. This type of behavior is not unexpected, and was observed in all simulations. It is also worthwhile noting that in all simulations the total head field exhibited behavior similar to that depicted in Figure

TABLE 4

Summary of Gridding Options and Porous Media Properties used in the Numerical Simulations.

a. Diagnostic Simulation Case Summary

Case I.D.	Spatial Discretization	Media Characteristics
1	Fine grid	Nonhysteretic and isotropic
2	Fine grid	Hysteretic and isotropic
3	Fine grid	Nonhysteretic, const. anisotropy = 1.5
4	Fine grid	Hysteretic, const. anisotropy = 1.5
5	Coarse grid	Hysteretic, const. anisotropy = 1.5
6	Fine grid	Nonhysteretic, variable anisotropy
7	Fine grid	Nonhysteretic, const. anisotropy = 10.0

b. Summary of Porous Media Properties

□ Flow Problem

k_{22} (minor axis of k_{sat} tensor) for all simulations		= 36 cm/hour
Effective porosity		= 0.35
Residual water saturation		= 0.18"
Variable anisotropy parameters (see eqn. 18)	σ^2_f	= 0.82
	σ^2_α	= 0.002
	λ	= 8 cm
	A	= 0.13
	$cos\ \beta$	= 1.0

□ Transport Problem

Longitudinal dispersivity in hydrodynamic dispersion	= 8.00 cm
Transverse dispersivity in hydrodynamic dispersion	= 1.00 cm

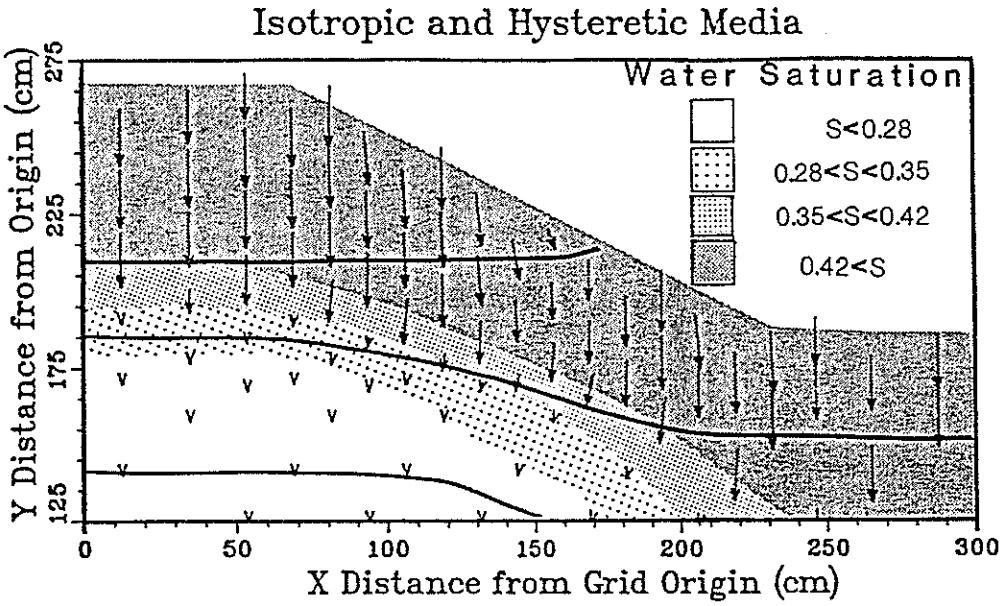

Figure 21. Velocity vector, total head, and water saturation fields for simulation Case 2 at t = 3.5 hours. Total head contour interval is 50 cm water.

21: a near unitary downward vertical gradient was observed at all times except near the wetting front early in the simulation, where the gradient had a slight component *into* the hillslope.

The simulated solute plume contours at t = 12 hours for Cases 1 and 2, presented in Figure 22, allow one to compare solute transport in hysteretic and nonhysteretic media with constant anisotropy. The hysteretic simulation exhibits a slightly larger downslope component to the soil water flux, as was predicted by McCord et al. (1989).

Nodal Spacing. Figure 23 provides a comparison of the fine grid versus coarse grid transport results given the same porous media properties (Cases 4 and 5) at t = 72 hours. Based on the position of the center of masses of the solute plumes, it is clear that the finer grid predicts a larger downslope flow component than does the coarse grid. Transport simulated using the coarse grid also contains a significant amount of numerical dispersion. Both of these features of Figure 23 we expected.

Variable Anisotropy. Figure 24 presents the solute plume development at various stages in time for the variable, state-dependent anisotropy simulation (Case 6). Only these results yield simulated solute plume behavior which appears similar to that which was observed in the field tracer experiments (Fig. 1). One can estimate effective macroscopic anisotropies of the media profile by applying the same simple Darcian considerations to the simulated plumes that were employed to estimate macroscopic anisotropies from the field tracer experiments (as discussed in the Field Investigation section). Table 5 summarizes the results of such anisotropy estimates for selected diagnostic simulations.

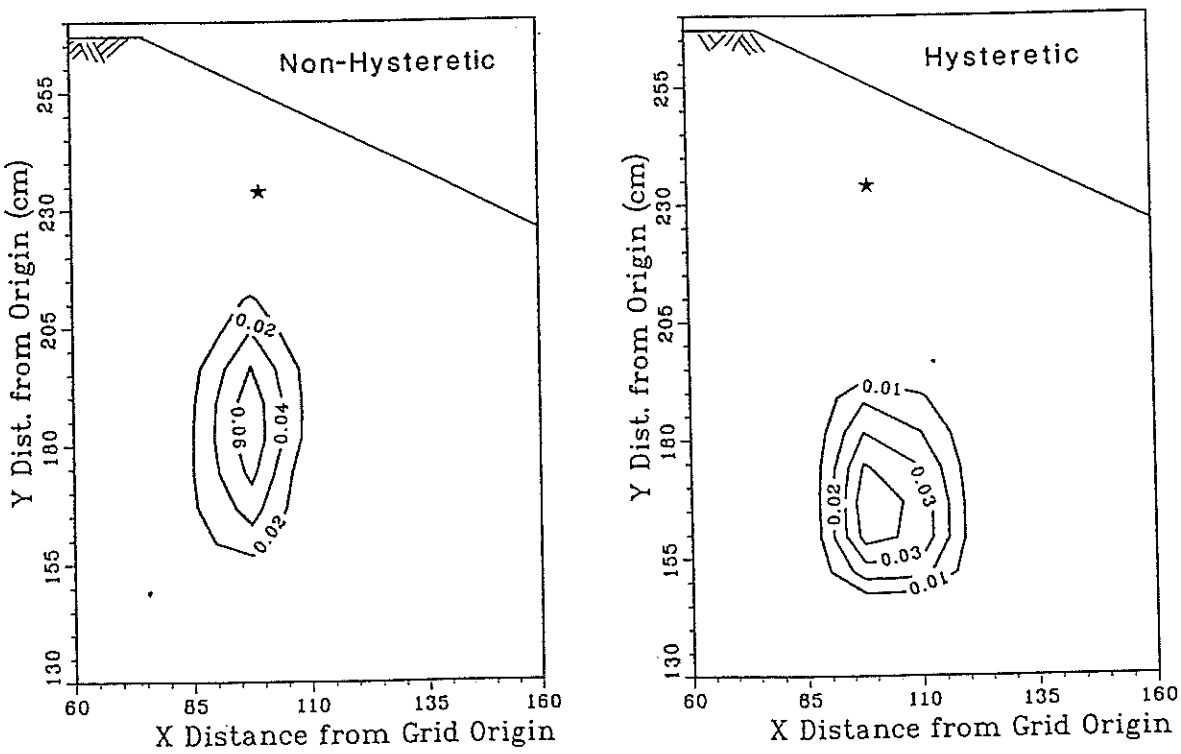

Fig. 22. Simulated solute plumes at t =12 hours for both non-hysteretic and hysteretic media with constant anisotropy ratio = 1.5:1 (simulation cases 3 and 4). Stars represent source locations.

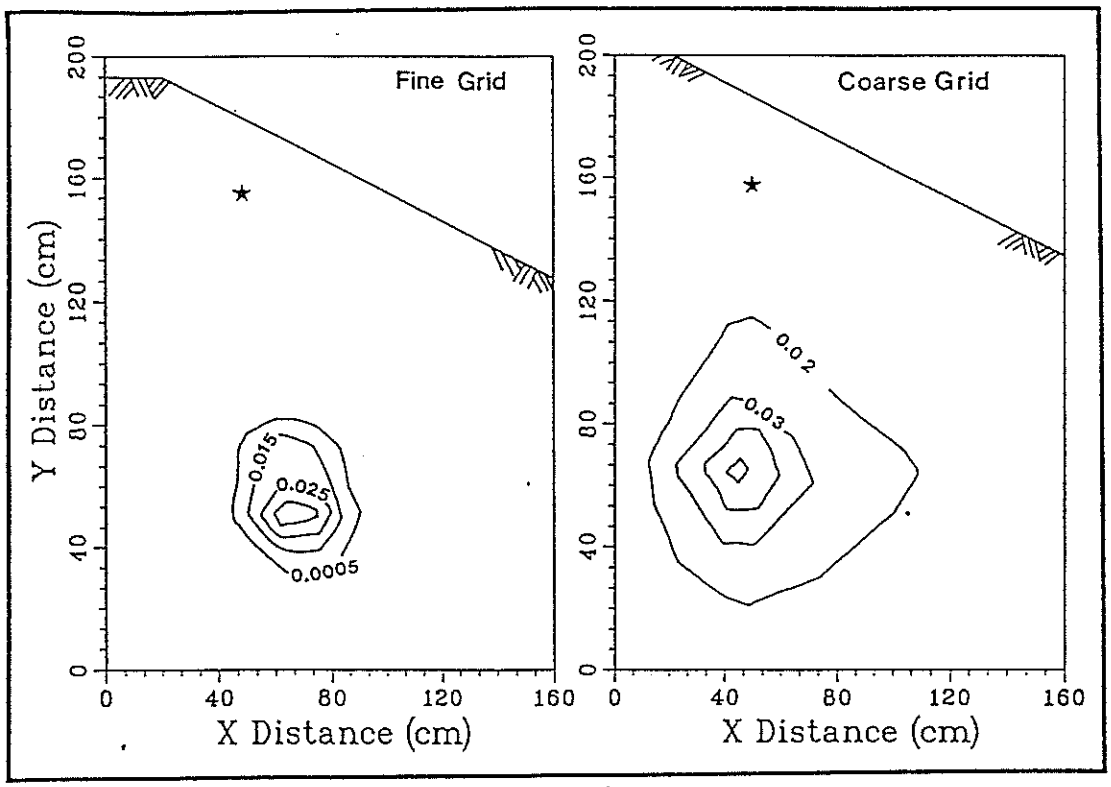

Fig. 23. Simulated solute plumes at t = 72 hours for fine and coarse grid simulations of flow and transport in hysteretic media with constant anisotropy ratio = 1.5:1 (simulation cases 4 and 5). Stars represent solute source locations.

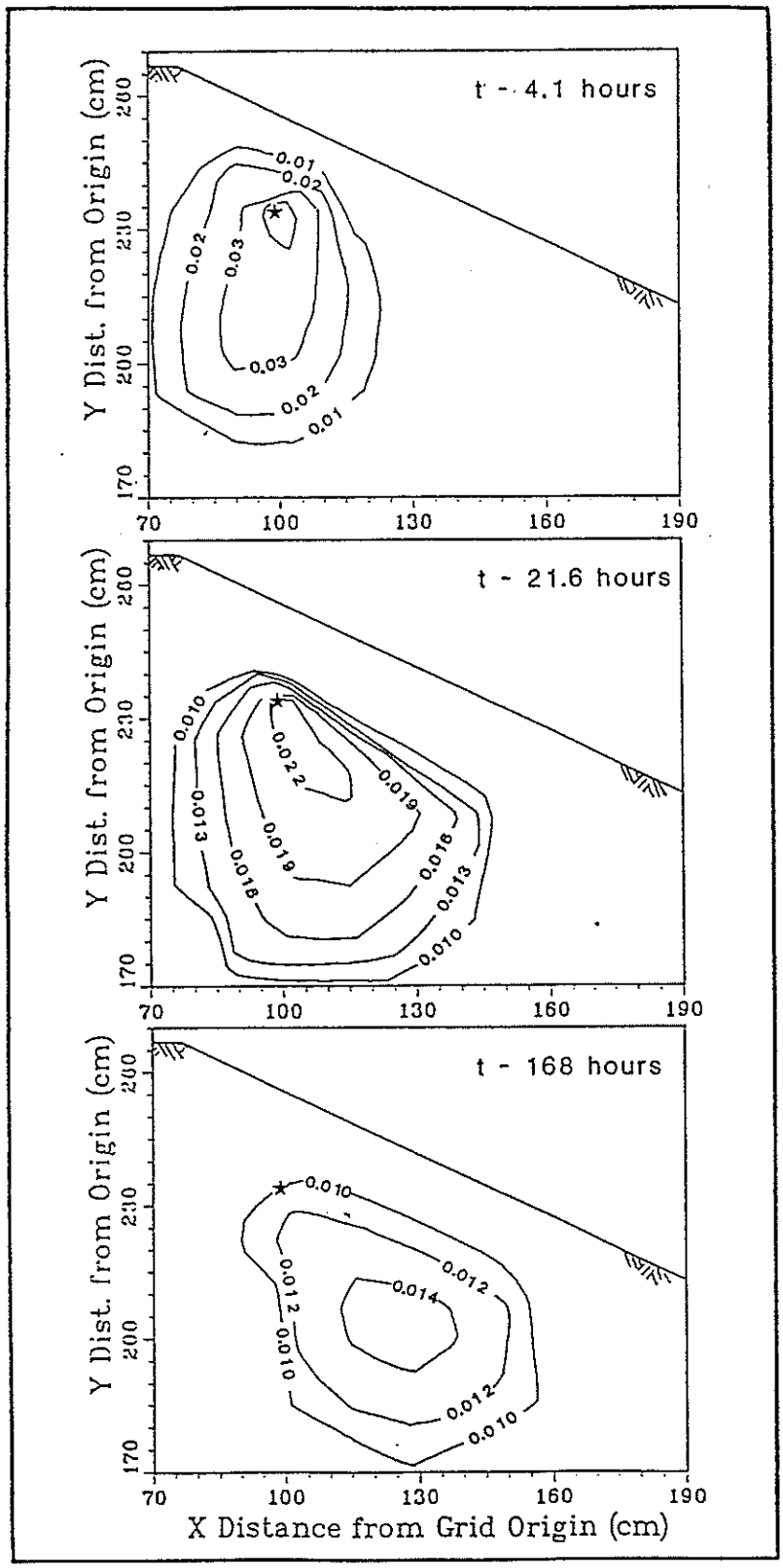

Fig. 24. Solute plume development at various times for simulation of flow and transport in non-hysteretic variable anisotropy media (simulation case 6). Stars represent solute source location.

TABLE 5

Macroscopic Anisotropy Estimates at Various Times for Selected Numerical Simulation Cases

Time Since Rainfall Began (hours)	Anisotropy Estimate for Simulation Cases			
	Case 3	Case 4	Case 5	Case 6
10	0.90	1.40	----	1.45
72	----	1.78	1.15	3.77
168	----	----	----	6.70

Based on the field tracer experiments the average anisotropy ratio of the sands *in situ* was estimated to be 10.4. Therefore one simulation was performed by specifying a constant anisotropy ratio = 10. In this simulation the directional saturated conductivities were specified such that their geometric mean ($\sqrt{k_{xx}k_{zz}}$) equalled the mean saturated conductivity determined in the laboratory permeameter analysis. The solute plume predicted for this run is shown at two different times in Figure 25. Clearly, specifying a large constant anisotropy equal to the average value estimated at the field site yields flow and transport predictions which significantly diverge from that which was observed. To aid in an interpretive comparison of the variable and constant anisotropy simulation results, we felt it would be useful to see how the anisotropy changed during the course of the variable anisotropy run. Figure 26 presents profile views of the variable anisotropy field at times plotted along with the unsaturated hydraulic conductivity field. Inspecting this plot provides an important clue as to why the constant anisotropy = 10 simulation yielded such unreasonable results: in the variable anisotropy simulation at early time anisotropy in the "zone of action" (high conductivity) region ranged between 1.5 and 4; only at later times did the anisotropy in the high K region exceed 5.

Summary of Diagnostic Simulation Results. Figures 21 through 25 show simulated solute plumes for a variety of gridding and material property options. Perhaps the most obvious (and most important) conclusion which can be drawn is that the simulation which accounts for textural heterogeneity induced state-dependent anisotropy does the best job at predicting transport behavior similar to that which was observed in the field experiments. Although the visual presentation of the plumes in these figures dramatically highlights the impact of considering variable anisotropy, quantitative analysis utilizing the locations

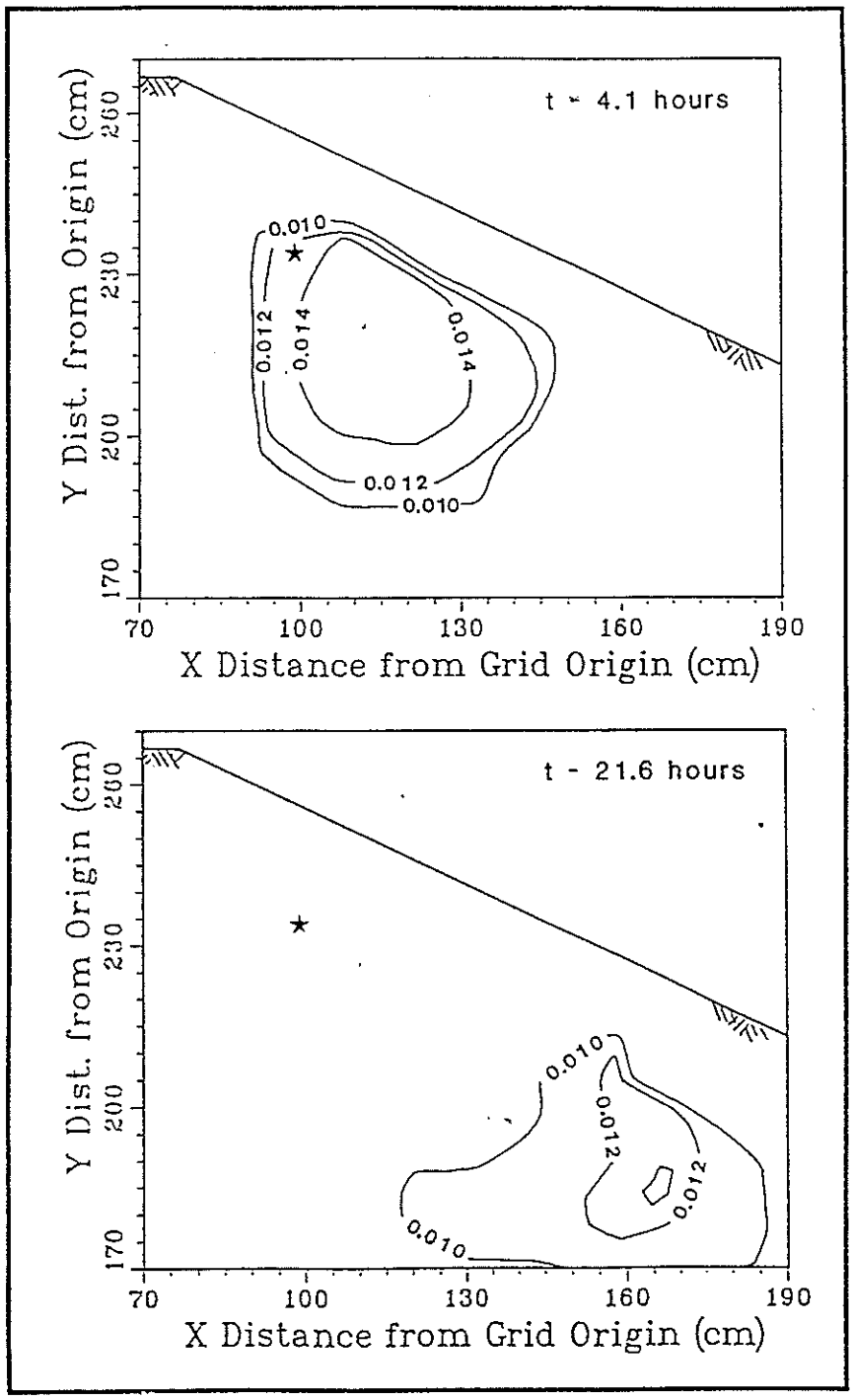

Fig. 25. Solute plume development at t = 4.1 hours and t = 21.6 hours for simulation of flow and transport in non-hysteretic media with a constant anisotropy ratio = 10:1 (simulation case 7). Stars represent solute source location.

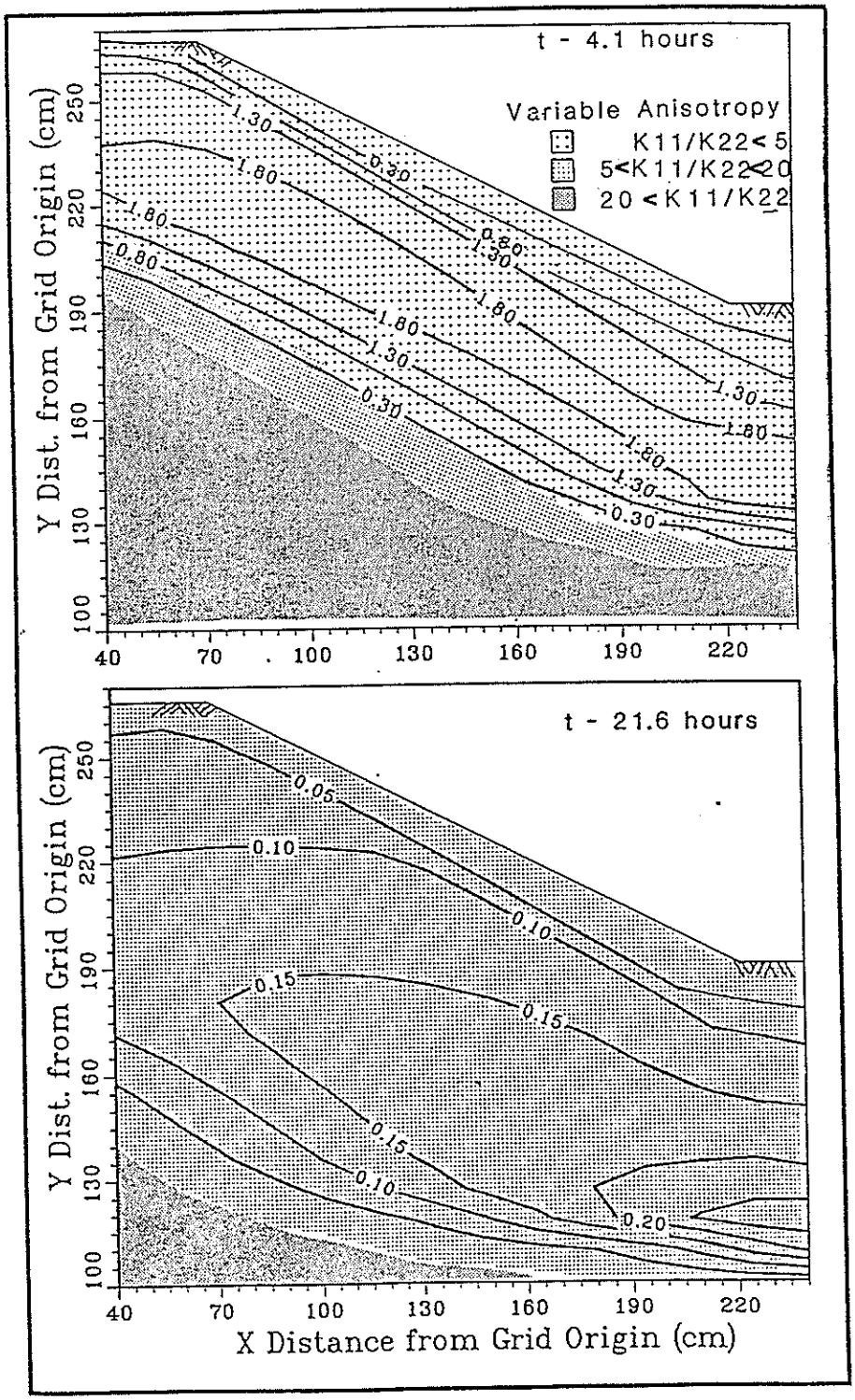

Fig. 26. Values of variable anisotropy function (K_{11}/K_{22}) and mean hydraulic conductivity (in cm/hour) at t = 4.1 hours and t = 21.6 hours for simulation case 6. Labeled contours are geometric mean conducitivity in cm/hour.

of the plume centroids provides a quantitative means of evaluating the subtle differences evidenced in the other plumes.

Table 5 presents macroscopic media anisotropies estimated from simulated plume geometries. Comparison of the hysteretic and non-hysteretic simulations at t = 10 hours suggest that hysteresis does enhance macroscopic anisotropic behavior, with the macroscopic anisotropy of the hysteretic media about 55% higher than that for the non-hysteretic media. Comparison of the fine and coarse grid simulations demonstrates that macroscopic anisotropy arising from moisture-dependent permeability variations can be modeled only by using a finely gridded spatial discretization, with the fine grid anisotropy (at t = 72 hours) more than 50% higher than that for the coarsely gridded system. These results coupled together suggest that hysteresis–enhanced moisture variations do indeed contribute to a macroscopic anisotropic behavior. Inspecting Figures 22 and 23, however, clearly illustrate that the magnitude of anisotropy predicted by the fine grid with hysteresis does not come close to that which was observed at the field site. It is likely that a further reduction in nodal spacing would result in even greater moisture content contrasts, and thus greater macroscopic anisotropies. However, trying to model anisotropy by such an approach would quickly become too much of a computational burden. And finally, Table 5 clearly shows that only for Case 6, the state-dependent anisotropy simulation, do the estimated macroscopic anisotropies come close to the values measured in our field experiments.

An important result (which has implications concerning the macroscopic anisotropies estimated from the field tracer experiments) is the fact that all of the macroscopic

anisotropies at times (t = 10 hours) are less than the local anisotropy specified as a material property (local anisotropy was specified to be 1.5). This should be expected, since this simple anisotropy estimation procedure assumes unit downward hydraulic gradient. Whereas in reality, at early times, capillary gradients will dominate and there will be a significant flow component normal to the ground surface slope. Therefore macroscopic anisotropies estimated from the field tracer experiments using this procedure may be somewhat on the low side.

For practical purposes, one might be interested in determining some "average" or "effective" constant anisotropy which could be used in predictive modeling of flow and transport, rather than having to modify an existing code to allow for variable anisotropy. To address such a question, we ran one simulation specifying a constant anisotropy ratio of 10:1 (near the average value estimated from the field tracer experiments). The results of this simulation, presented in Figure 25, clearly show that this approach predicts flow and transport behavior far different from that observed. To aid in the interpretation of this result, the anisotropy and hydraulic conductivity fields from the variable anisotropy simulation are plotted up for two different instances in time in Figure 26. Note that most of the significant flow occurs in the regions of highest hydraulic conductivity (or highest moisture content, since conductivity increases with saturation); one can refer to these areas as the "zones of action." Figure 26 illustrates that at early time, the anisotropy ratio in the zone of action is relatively low (less than 4:1). This early time behavior is rather transient, and at later times anisotropy ratios are higher in the zone of action. This state dependence of the anisotropy field results in the plume behavior shown in Figure 24, where at early time the plume suggests advection into the hillslope face, and

at later times the plumes indicate that the flux direction rotates in a downslope direction due to the increased anisotropy. The constant anisotropy case (Fig. 25), however, shows water moving rapidly downslope right from the beginning. The relatively small vertical conductivity inhibits the wetting front from propagating into the soil, and causes the development of a relatively moist (highly conductive) zone in the shallow soils. In contrast to the variable anisotropy case, however, the very wet surface soil (the zone of action) is highly anisotropic. Clearly, although such a simplified constant anisotropy approach is practically desirable, it seems to be physically unrealistic.

Sensitivity Simulations

The following set of results are from the simulations designed to examine the effect of precipitation intensity, geologic structure, and soil lithology. Based on the results of the diagnostic simulations in conjunction with the field experiment results, it is apparent that variable anisotropy is indeed a real phenomenon which plays a significant role in the flow and transport behavior at the Sevilleta field site. Therefore variable anisotropy was specified in all of the following model runs.

Precipitation Intensity. Solute plume development for the low intensity, long duration rainfall case can be found in Figure 27. As might be expected, the solute plume shows smaller overall transport distance, but a larger macroscopic anisotropy (as evidenced by the flux distance parallel to the slope divided by the flux distance normal to the slope) than that predicted in the variable anisotropy simulation with high intensity rainfall. This was expected since anisotropy tends to decrease with increasing wetness. This result suggests that in a natural field setting at a site underlain by sloping layered soils, only

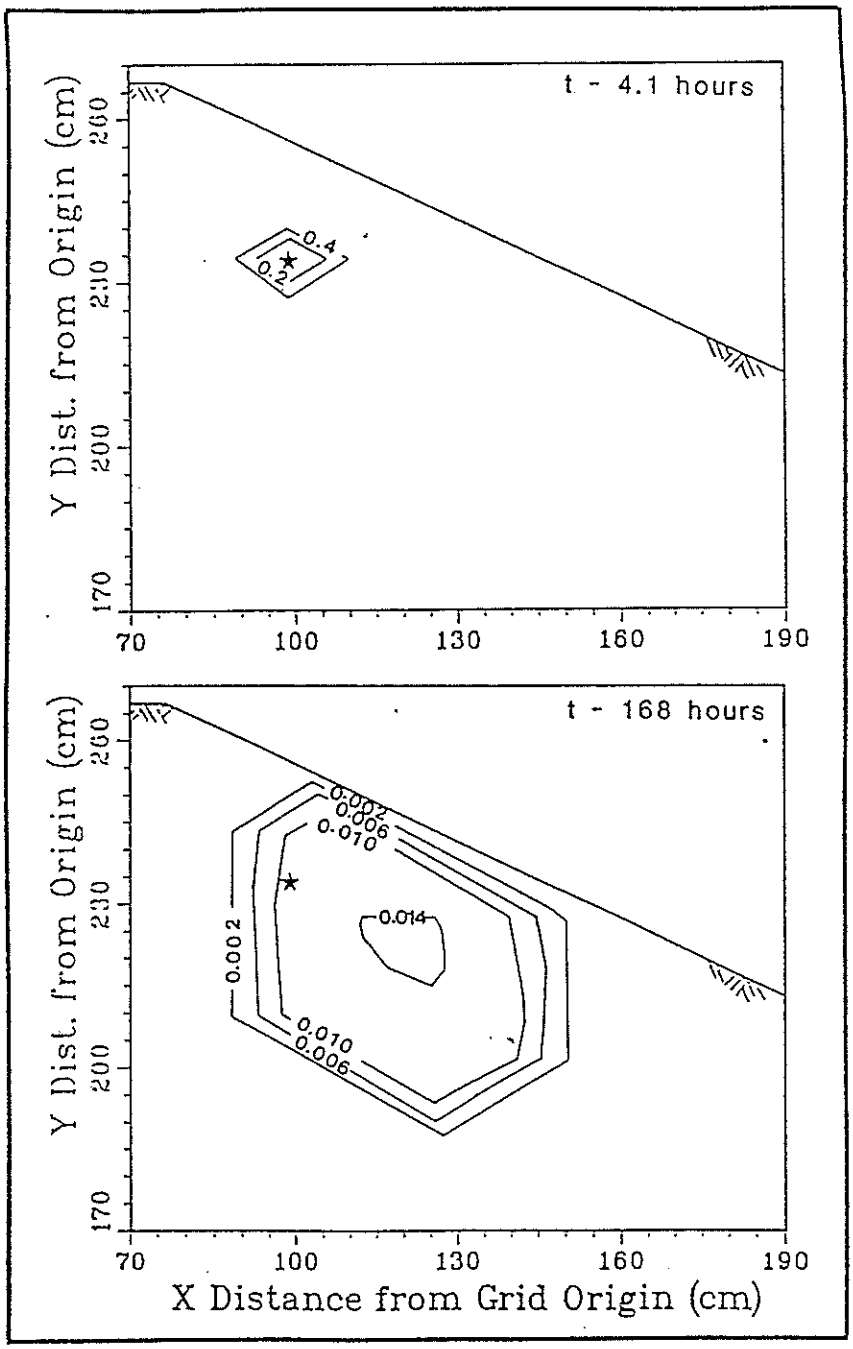

Fig. 27. Solute plume development at t = 4.1 hours and t = 168 hours for simulation of flow and transport in variable anisotropy Sevilleta dune sands following long duration, low intensity precipitation event.

relatively intense precipitation events (relative to the soil's saturated conductivity) will cause the advection of water into the deep subsoils, except at the hillslope base.

Media Orientation. The importance of dip (slope direction) of the porous media stratifications is demonstrated in Figure 28, which shows resultant solute plumes at the end of one week following a high intensity rainfall for the case of horizontally stratified media, and the case of media which dips into the hillslope at angle of 22 degrees. Not surprisingly, the resulting solute plumes suggest a significant component of the soil water flux is in the direction parallel to the media stratifications. Recall that for all of the diagnostic simulations (see previous section) the soil strata were specified to be oriented with the ground surface slope. If such behavior is true for porous materials in general, including geologic media such as sandstone, this could have important implications for processes such as groundwater recharge in outcrop areas of aquifers.

Hillslope Angle. Figure 29 shows solute plume movement for a long duration, low intensity rainfall event (4 cm in 12 hours) on a relatively mild hillslope composed of the Sevilleta dune sands. The ground surface slope for this case was only 7.5° whereas the ground surface slope in all preceding simulations was 22°. The plumes clearly indicate significant downslope flow components in spite of the gentle topographic slope. These lateral flow components lead to the development of moisture concentrations at the base of the slope, as demonstrated by Figure 30. Such base-of-hillslope moisture content concentrations were clearly documented in a study by McCord and Stephens (1987).

Soil Lithology. To investigate the role of soil type, we wanted to contrast our simulations of flow through the Sevilleta sands with a simulation considering flow and transport be-

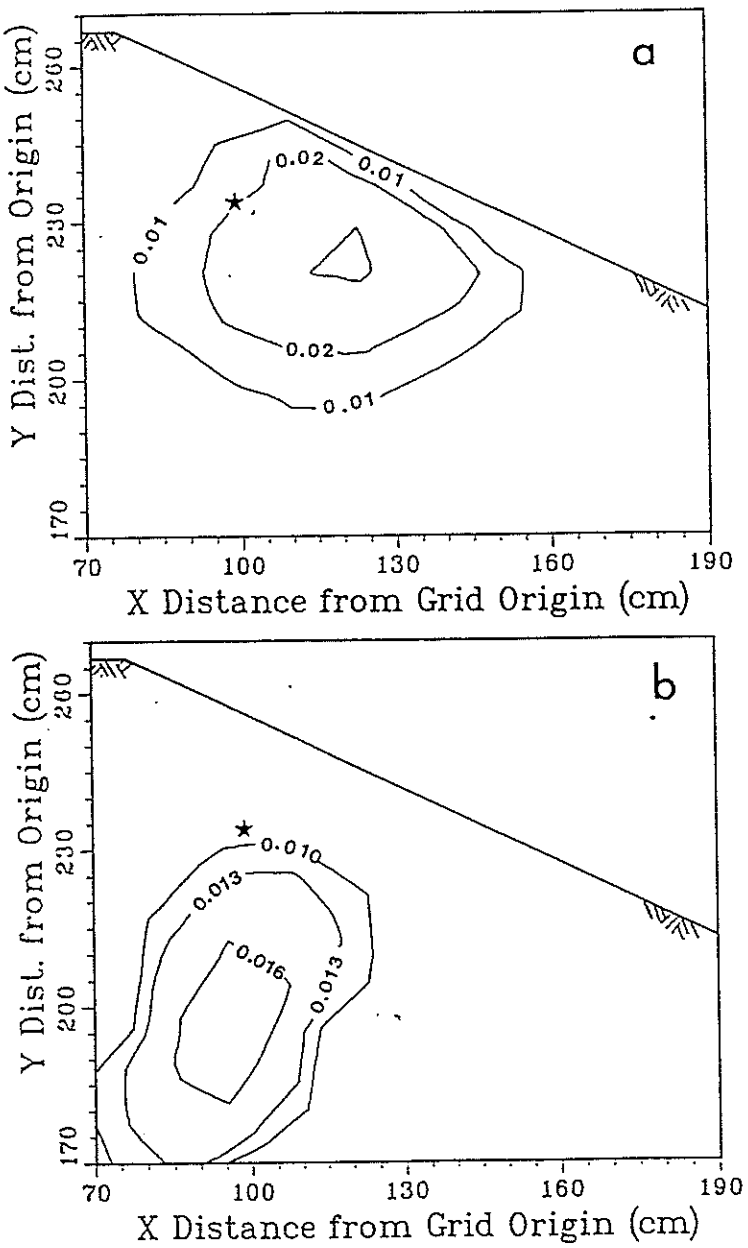

Fig. 28. Solute plume at t = 168 hours in (a) horizontally stratified dune sand, and (b) dune sand with stratifications which dip 22° into the hillslope.

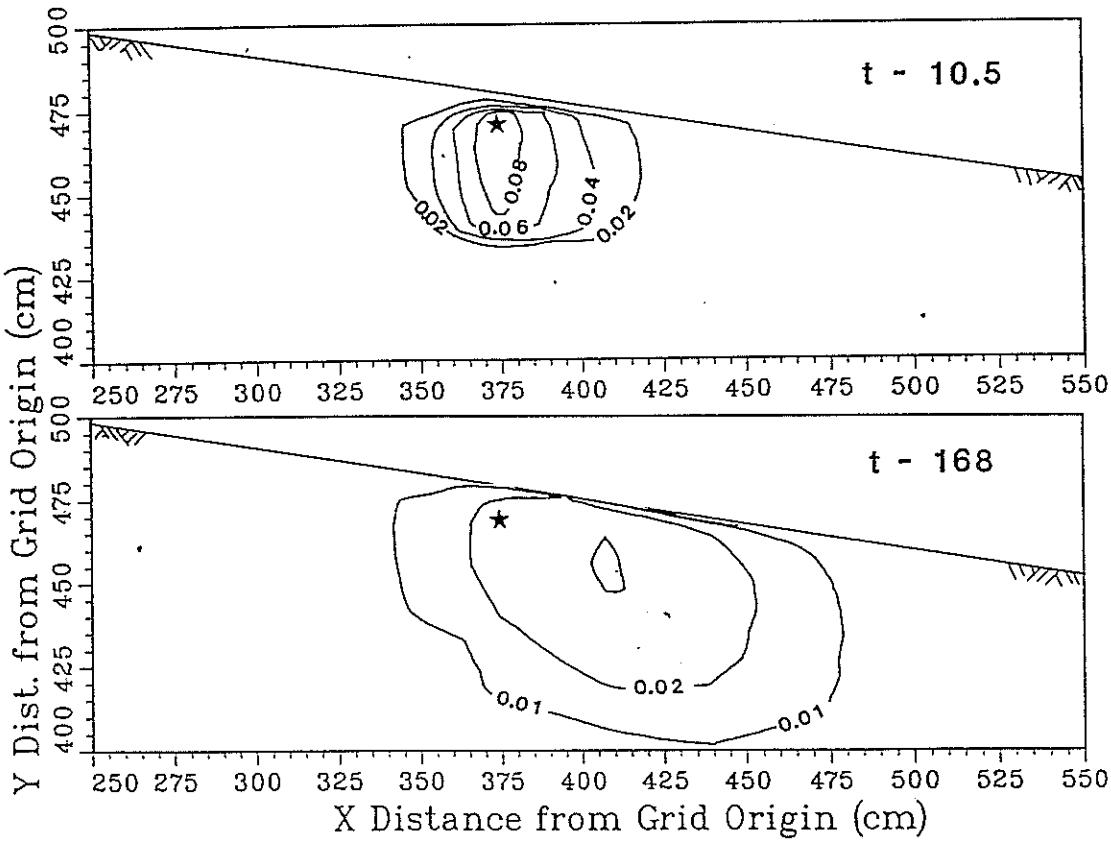

Fig. 29. Solute plume at t = 10.5 hours and t = 168 hours for simulation of flow and transport in a gentle hillslope composed of Sevilleta dune sands. Stars represent solute source location.

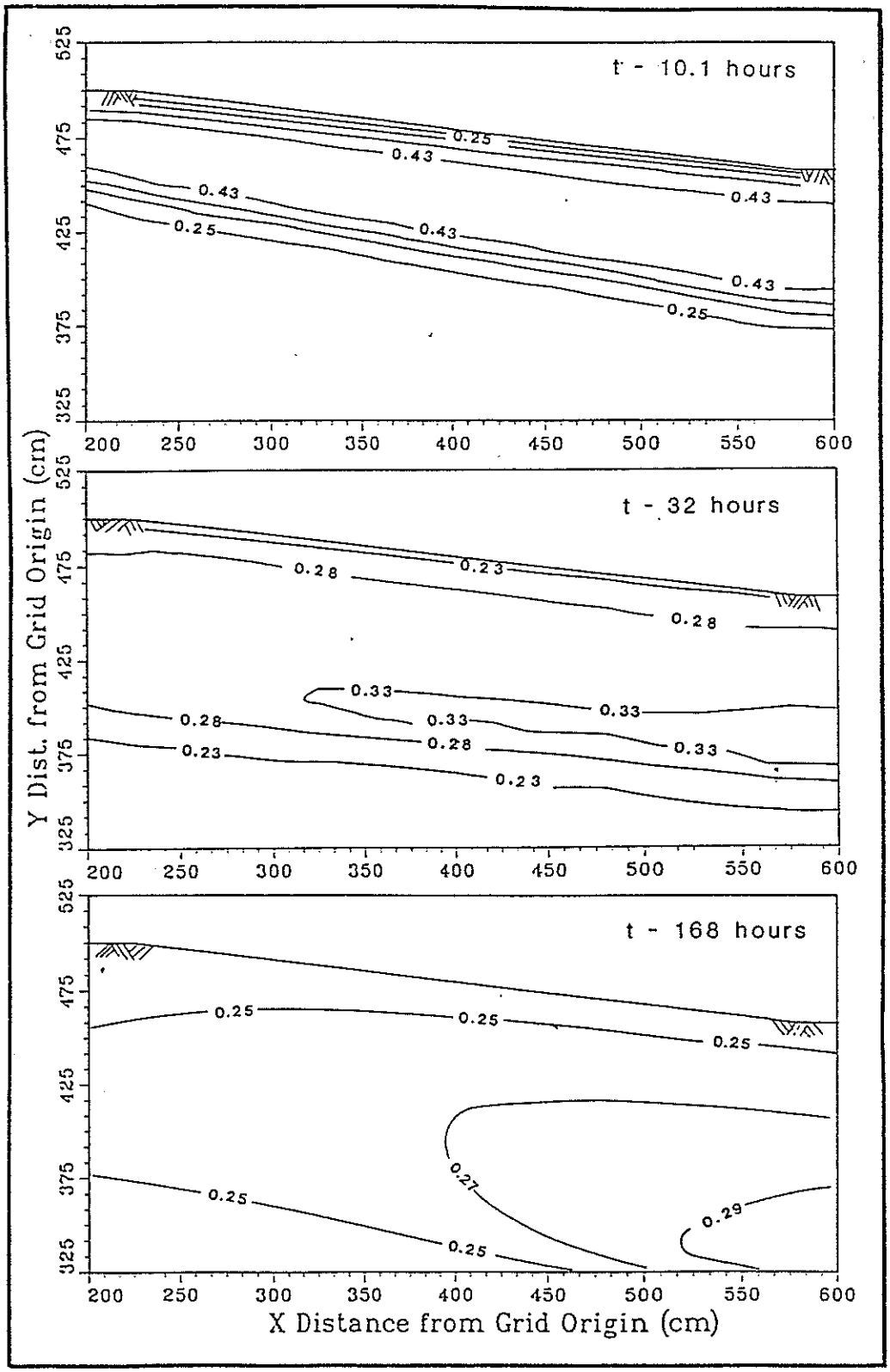

Fig. 30. Water saturation profiles at t = 10.1, t = 32, and t = 168 hours for gentle hillslope composed of Sevilleta dune sands with variable anisotropy

neath a hillslope composed of a clayey material. Nielsen et al. (1978) studied the spatial variability in the hydraulic properties of the Panoche clay loam. This large data base permitted calculation and/or estimation of the various statistical parameters required as input for the stochastic variable anisotropy model. Therefore, we performed one final simulation which looked at the response of the gentle (7.5^o) hillslope underlain by Panoche clay loam. Input parameters for the Panoche soil are listed in Table 6. This hypothetical hillslope was subjected to the same long duration, low intensity rainfall as specified for the gentle slope composed of Sevilleta dune sands. Figure 31 present solute plume development for this situation. This figure indicates that the Panoche soils should behave much less anisotropically than the Sevilleta sands. The primary transport direction through the Panoche profile appears to be vertical downward. Both Mualem (1984) and the stochastic researchers (Yeh, et al., 1985b; Mantoglou and Gelhar, 1987c) predicted that finer materials would behave less anisotropically than coarse granular soils. In this case the smaller macroscopic anisotropy of the Panoche clay loam is due primarily to the much smaller ${\sigma^2}_\alpha$ (variance of the slope of the $lnK - \psi$ relationship).

Summary of Modeling Results

Taken all together, the diagnostic numerical simulations indicate that for the Sevilleta dune sands capillary hysteresis is of minor importance compared to textural heterogeneity in causing macroscopic variable anisotropy in unsaturated media. These results strongly support the stochastic theory results (Yeh et al., 1985b,c; Mantoglou and Gelhar, 1987c) which indicate a strong dependence of the macroscopic anisotropy on the hydraulic state (primarily the mean pressure head) of the media. The sensitivity simulations suggest that both soil type and dip direction of layered porous materials strongly affect unsaturated

TABLE 6

Hydraulic and Stochastic Properties used for Panoche Clay Loam Simulations (from Nielsen et al., 1976; Mantoglou and Gelhar, 1987b)

Parameter	Value
k_{sat}	2.00 (cm/hr)
A	0.0294 (1/cm)
σ^2_f	2.48
σ^2_α	0.000067
λ_1	100.00 (cm)

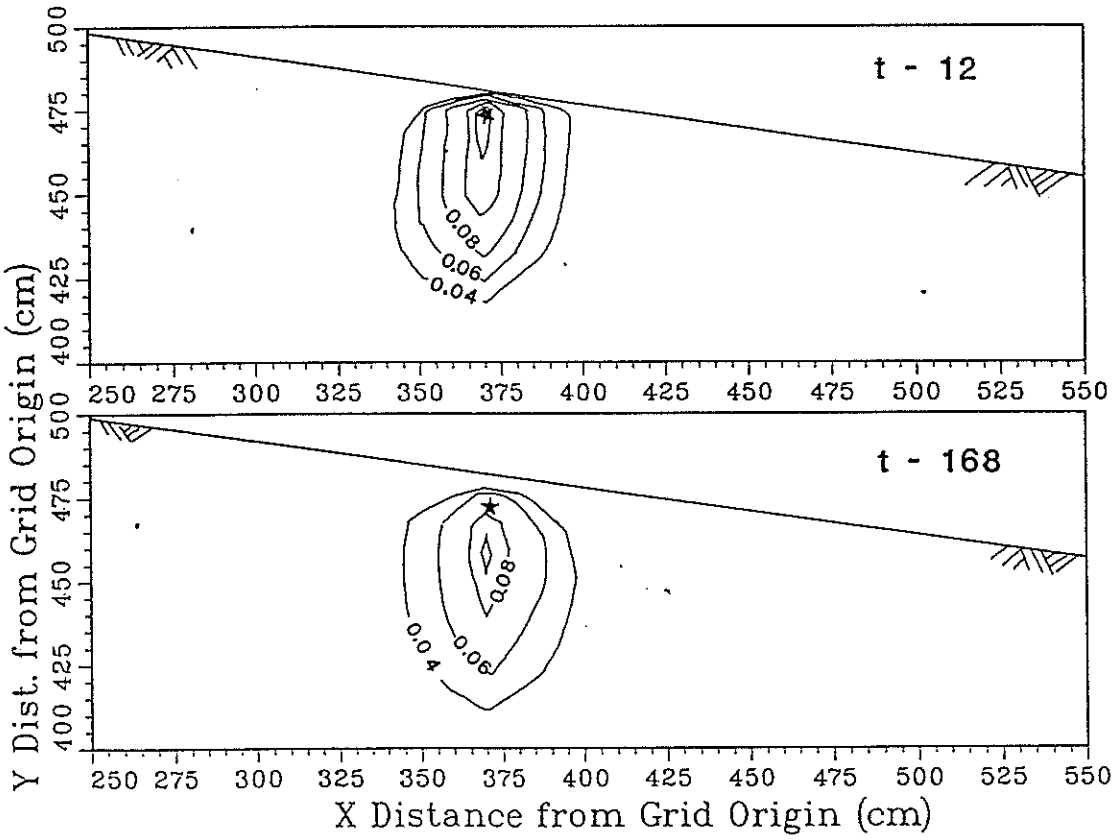

Fig. 31. Solute plume at t = 12 hours and t = 168 hours for simulation of flow and transport in a hillslope composed of Panoche clay loam. Stars represent solute source location.

flow and transport behavior.

PRACTICAL IMPLICATIONS

The first practical implication of these results is that state-dependent anisotropy, a media property which has been proposed in recent theoretical studies, is indeed a real and significant phenomenon in some natural landscapes at field scales. Since in general anisotropy increases with dryness, this phenomenon should be particularly important in relatively dry regions with deep water tables. At these locations shallow subsurface water movement occurs primarily as an unsaturated process. Given the potential for orders of magnitude variation in hydraulic anisotropy, this can have important consequences on our understanding of any number of processes, from ground-water recharge and watershed hydrology to erosion and gully formation; from hazardous waste containment by burial to stability of natural and engineered slopes.

Consider, for instance, natural ground-water recharge. In a natural field setting, shallow soils exhibit varying degrees of heterogeneity. The relatively uniform Sevilleta dune sands might be considered to be quite homogeneous when compared to soils encountered at other locations. One would expect soils with a greater layered heterogeneity to exhibit a larger macroscopic anisotropy than the Sevilleta sands, and thus unsaturated flow paths would have a significant component in the dip direction of the media stratification. In topographically variable terrain, when dip direction is oriented in roughly the same direction as the topographic slope (which would generally be true for areas with developed soil profiles), lateral unsaturated fluxes would be primarily downslope and would result

in base of hillslope moisture concentrations (Fig.20). Recalling the variable anisotropy models, the wetter soils at the hillslope base would be less anisotropic. Under predominantly vertical, gravity-dominated hydraulic gradients, downward vertical flow (in effect, recharge rates) would be enhanced at the base of hillslopes.

Besides enhancing groundwater recharge for this scenario, such moisture concentrations greatly impact other surficial hydrologic processes as well. For instance, under rainfall infiltration, the relatively high antecedent moisture content of the soils at the hillslope base will result in a significantly reduced time to saturation and subsequent runoff generation (McCord and Searcy, 1989). Therefore, rainfall-runoff models which fail to account for the uneven antecedent moisture distribution will predict times to runoff generation which are much longer than those predicted if variable anisotropy is considered. This reduced time to ponding and runoff generation may also impact our understanding and predictive modeling of erosion and gully formation. Anisotropy-induced base of hillslope moisture concentrations can also affect soil strength, and thus have implications for stability analysis of natural and engineered slopes.

Now consider a contrasting scenario in which media stratifications dipped into the hillslope face. This is the type of setting one would expect, say, for a resistant rock (such as sandstone) which outcrops on a slope face. This type of geologic setting can be found all across the planet in rocky terrains, and is readily observed in the arid and semi-arid regions of the western United States. Figure 28 depicts unsaturated transport behavior for such a configuration. The implied flow components into the hillslope face may provide additional support for the unproven hypothesis of aquifer recharge occurring

in the outcrop zone of aquifers (Stephens, 1983) in the Colorado Plateau of western North America.

Another practical implication lies in mathematical modeling of variably saturated flow and transport. If variable anisotropy is an actuality, then widely used quantitative modeling approaches are deficient in this respect. Analytical solutions for unsaturated flow problems may be even more difficult to obtain, and numerical flow models may require modifications to allow for consideration of a state–dependent anisotropy. The modeling results in this paper clearly show the dramatic difference in predicted flow and transport behavior depending on whether or not variable anisotropy is accounted for. It is important that the modeler recognize that variable anisotropy is a large-scale effective parameter resulting from textural media heterogeneities at smaller scales, and that the large-scale governing equation (eqn. 11) will describe only mean behavior. One may think that accounting for variable macroscopic anisotropy in a model increases data requirements because geostatistical descriptors of the spatial variability in the soil hydraulic properties are needed. However, to capture the fine-scale behavior (which results in the macroscopic anisotropy) using the conventionally parameterized Richards equation, one would need to deterministically describe and simulate all of the small-scale heterogeneities. Thus, although a large number of measurements may be required to estimate the large-scale parameters, overall data requirements may actually be reduced.

These results suggest the need for additional research on this topic. These results do not necessarily mean that everyone who models unsaturated flow and transport should automatically go out and modify their predictive codes to include variable anisotropy as we

have implemented it. The study is simply another step in the important validation process for the stochastic models. Our results certainly provide substantial support to the variable anisotropy theory, and they demonstrate that it can be included in a flow simulator by implementing some fairly minor (with respect to coding) modifications. The theory, however, represents a fairly significant step in our conceptualization of the unsaturated flow process. Therefore, it is imperative that more large-scale field experiments (such as those described by Wierenga et al., 1988; and Stephens et al., 1988) and/or laboratory experiments be designed and performed to determine if this phenomenon is important for a wide variety of soil types. Tests should also be performed to assess the applicability of the analytical stochastic results in the dry range (see discussion by McCord [1988]). Detailed Monte Carlo simulations of flow through layered materials which are currently being performed by the first author should help answer some of these questions. The Monte Carlo work of Hopmans et al. (1988) represents an important contribution in this regard, but it does not fully address the importance of layering. We should also re-examine the methods used to characterize the hydraulic properties of porous media, and how local (laboratory scale) measurements should be incorporated into large scale models.

SUMMARY

Detailed soil–water tracer experiments conducted on a sand dune indicate that significant horizontal downslope flow components develop despite the presence of a near vertical downward hydraulic gradient. This suggests that at *in situ* pressure heads (-30 to -80 cm) the dune sands behave as a highly anisotropic medium. Field and laboratory permeameter analyses show that the sands are nearly isotropic at complete saturation. These field and laboratory measurements provide strong supporting evidence for the theoretical (Mualem, 1984; Yeh et al., 1985b, c) and experimental (Bear et al., 1987; Stephens and Heermann, 1988) postulations that anisotropy in hydraulic conductivity of unsaturated heterogeneous porous media varies as the state (capillary pressure, saturation, . . .) of media varies. Simple arguments developed herein show that moisture content heterogeneities in a texturally uniform homogeneous medium can cause the medium to behave anisotropically with respect to fluid flow. Hysteresis in the soil moisture characteristics should slightly enhance the macroscopic anisotropy of a texturally homogeneous medium.

Three different approaches were taken to model the flow and transport observed at our field site: constant anisotropy with no hysteresis, constant anisotropy with hysteresis, and state dependent anisotropy without hysteresis. Results of the numerical simulations demonstrate that hysteresis enhanced moisture–dependent permeability variations do contribute slightly to the macroscopic anisotropy evidenced at the field site. To successfully model these contributions the spatial domain must be finely discretized. However, only the simulation which accounted for state–dependent, variable anisotropy predicted downslope flow and solute transport behavior which was similar to that observed in the field

experiments. These significant lateral flows were modeled using nodal spacings which were not unreasonably small, which suggests that the variable anisotropy approach may be well suited to modeling field–scale problems.

In summary, the results of this study indicate that state–dependent anisotropy in hydraulic conductivity and, to a much smaller extent, hysteresis in the soil–moisture characteristics are important phenomena which can have dramatic implications on our understanding and mathematical modeling of field scale flows in variably saturated media.

REFERENCES

Andersson, J., and A.M. Shapiro. 1983. Stochastic Analysis of one-dimensional steady state unsaturated flow: A comparison of Monte Carlo and perturbation methods, Water Resour. Res., V.19(1):121-133.

Bear, J., C. Braester, and P. Menier. 1987. Effective and relative permeabilities of anisotropic porous media, Transport in Porous Media, V.2:301-316.

Bear, J., and C. Braester. 1987. Comment on "A three-dimensional finite element model for simulating water flow in variably saturated porous media," by P.S. Huyakorn et al., Water Resour. Res., V.23(8):1705-1706.

Bouwer, H. 1969. Infiltration of water into nonuniform soil, J. Irr. Drain., Div., ASCE 95(IR4):451-462.

Burden, R.L., and J.D. Faires. 1985. Numerical Analysis, 3rd Edition, PWS Publishers, Boston, 675 pp.

Byers, E., and D.B. Stephens. 1983. Statistical and stochastic analyses of hydraulic conductivity and particle size in a fluvial sand, Soil Sci. Soc. Amer. Proc., 47(6):1072-1080.

Dagan, G., and E. Bresler. 1983. Unsaturated flow in spatially variable fields, 1. Derivation of models of infiltration and redistribution, Water Resour. Res., V.19(2):413-420.

Dettinger, M.D., and J.L. Wilson. 1981. First-order analysis of uncertainty in numerical methods in groundwater flow, Water Resources Res., V.17(1):149-161.

Freeze, R.A., and J.A. Cherry. 1979 Groundwater, Prentice-Hall, Englewood Cliffs, NJ, 604 pp.

Freyburg, D.L. 1986. A natural gradient tracer experiement on solute transport in a sand aquifer, 2. Spatial moments and the advection and dispersion of nonreactive tracers, Water Resour. Res., V.22(13):2031-2046.

Hanks, R.J., A. Klute, and E. Bresler. 1969. A numeric method for estimating infiltration redistribution, drainage, and evaporation of water from soil, Water Resour. Res., V.5(5):1064-1069.

Hopmans, J.W., H. Schukking, and P.J.J.F. Torfs. 1988. Two-dimensional steady state unsaturated water flow in heterogeneous soils with autocorrelated soil hydraulic properties, Water Resources Res., V.24(12):2005-2017.

Huyakorn, P.S., S.D. Thomas, and B.M. Thompson. 1984. Techniques for making finite elements competitive in modeling flow in variably saturated porous media, Water Resour. Res., V.20(8):1099-1115.

Huyakorn, P.S., J. Kool, and H. White. 1989. VAM2D: A variably saturated analysis model with hystersis and anisotropy in two-dimensions, NUREG/CR-5352, HGL/89-01.

Jaynes, D.B. 1984. Comparison of soil-water hysteresis models, Journal of Hydrology, V.75:287-299.

Leavitt, M.L. 1987. Spatial variability of soil hydraulic parameters at the Sevilleta National Wildlife Refuge, M.S. Thesis, New Mexico Institute of Mining and Technology.

Lumley, J.L., and H.A. Panofsky. 1974. The Structure of Atmospheric Turbulence, John Wiley, New York.

McCord, J.T. 1988. Hysteresis and State-Dependent Anisotropy in Variably Saturated Flow: Field, Laboratory, and Numerical Modeling Investigation, Ph.D. Dissertation, New Mexico Institute of Mining and Technology, Socorro, 180 pp.

McCord, J.T., and C.C. Searcy. 1989. Impact of soil heterogeneity on antecedent moisture and runoff generation at an arid site, EOS Trans. AGU, V. 70(15):343.

McCord, J.T., and D.B. Stephens. 1987. Lateral moisture movement on sandy hillslope in the apparent absence of an impeding layer, Journal of Hydrological Processes, V.1(3):225-228.

McCord, J.T., D.B. Stephens, and J.L. Wilson. 1989. Toward validating variable macroscopic anisotropy in layered unsaturated media: Field experiments and modeling considerations, in press, Journal of Contaminant Hydrology.

Mantoglou, A., and L.W. Gelhar. 1987a. Stochastic modeling of large-scale transient unsaturated flow systems, Water Resour, Res., V. 23(1):37-46.

Mantoglou, A., and L.W. Gelhar. 1987b. Capillary tension head variance mean soil moisture content, and effective soil moisture capacity of transient unsaturated flow in stratified soils, Water Resour. Res., V. 22(1):47-56.

Mantoglou, A., and L.W. Gelhar. 1987c. Effective hydraulic conductivities of transient unsaturated flow in stratified soils, Water Resour. Res., V. 23(1):57-68o.

Mualem, Y. 1984. Anisotropy of unsaturated soils, Soil Sci. Soc. of Amer. Journal, V.48:505-509.

Nielsen, D.R., J.W. Biggar, and K.T. Erh. 1973. Spatial variability of field-measured soil-water properties, Hilgardia, V.42(7):216-259.

Philip, J.R. 1974. Recent progress in the solution of nonlinear diffusion equations, Soil Science, V.117:257-264.

Polmann, D.J., E.G. Vomvoris, D. McLaughlin, E.M. Hammick, and L.W. Gelhar. 1988. Application of stochastic methods to the simulation of large-scale unsaturated flow and transport, NUREG/CR-5094.

Rubin, J. 1967. Numerical method of analyzing hysteresis affected post-infiltration redistribution of soil moisture, Soil Sci. Soc. of Amer. Proc., V.31:13-20.

Stephens, D.B. 1983. Groundwater flow and implications for groundwater contamination north of Prewitt, New Mexico, U.S.A., Journal of Hydrology, V.61:391-408.

Stephens, D.B., and S. Heerman. 1988. Dependence of anisotropy on saturation in a stratified sand, Water Resour. Res., V.24(5):770-778.

Stephens, D.B., A.M. Parsons, E.D. Mattson, K. Black, K. Flanigan, R.S. Bowman, and W.B. Cox. 1988. A field experiment of three-dimensional flow and transport in a statified soil, in Proc. Validation of Flow and Transport Models for the Unsat. Zone, Research Report 88-SS-04:401-413, Dept. of Agronomy, New Mex. State Univ., Las Cruces, NM.

van Genuchten, M.Th. 1980. A closed-form equation for predicting the hydraulic conductivity of unsaturated soils, Soil Sci. Soc. of Amer. Journ., V.44:892-898.

Wierenga, P. J., et al. 1988. Validation of stochastic flow and transport models for unsaturated soils, Research Report 88-SS-03, Department of Agronomy and Horticulture, NMSU, Las Cruces.

Yeh, T.-C., Analysis of one-dimensional steady infiltration in heterogeneous soils, in Proc. Validation of Flow and Transport Models for the Unsat. Zone, Research Report 88-SS-04:539-547, Dept. of Agronomy, New Mex. State Univ., Las Cruces, NM, 1988.

Yeh, T.-C., Jim, L.W. Gelhar, and A.L. Gutjahr, Stochastic analysis of unsaturated flow in heterogeneous soils; 1. Statistically isotropic media, Water Resour. Res., V. 21:447-456, 1985a.

Yeh, T.-C., Jim, L.W. Gelhar, and A.L. Gutjahr, Stochastic analysis of unsaturated flow in heterogeneous soils; 2. Statistically anisotropic media with variable a, Water Resour. Res., V. 21:457-464, 1985b.

Yeh, T.-C., Jim, L.W. Gelhar, and A.L. Gutjahr, Stochastic analysis of unsaturated flow in heterogeneous soils; 3. Observations and applications, Water Resour. Res., V. 21:465-471, 1985c.

Yeh, T.-C., L.W. Gelhar, and P.J. Wierenga. 1986. Observations of spatial variability of soil-water pressure in a field soil, Soil Sci., V.142(1):7-12.

Zaslavsky, D., and G. Sinai. 1981a. Surface hydrology: I - Explanation of Phenomena, Journal of the Hydraulics Division, ASCE, V. 107, No. HY1, Proc. Paper 15959, pp. 17-35.

Zaslavsky, D. and G. Sinai. 1981c. Surface hydrology: III - Causes of Lateral Flow, Journal of the Hydraulics Division, ASCE, V. 107, No. HY1, Proc. Paper 15960, pp. 53-64.

Zaslavsky, D. and G. Sinai. 1981d. Surface hydrology: IV - Flow in Sloping, Layerd Soil, Journal of the Hydraulics Division, ASCE, V. 107, No. HY1, Proc. Paper 15961, pp. 53-64.

Zaslavsky, D. and G. Sinai. 1981e. Surface Hydrology: V - In-Surface Transient Flow, Journal of the Hydraulics Division, ASCE, V. 107, No. HY1, Proc. Paper 15962, pp. 65-93.